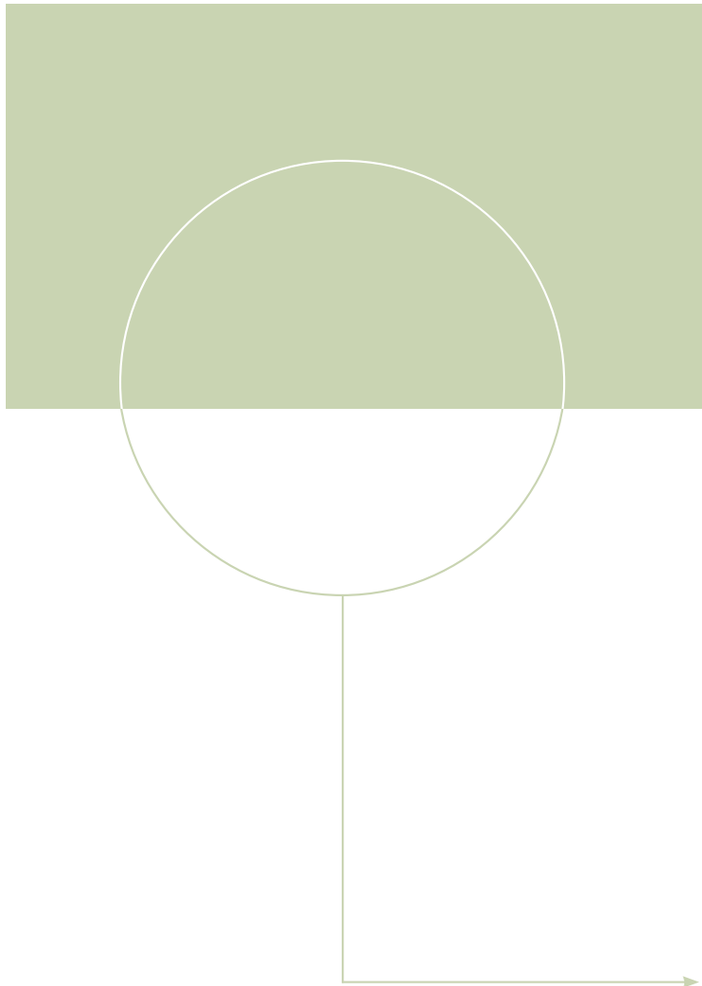

Master's thesis

2019

Ingeborg Dahl

NTNU
Norwegian University of
Science and Technology
Faculty of Natural Sciences
Department of Chemical Engineering

Ingeborg Dahl

Experiments on Single Droplet Breakage in Turbulent Flow

July 2019

NTNU
Norwegian University of
Science and Technology

NTNU
Norwegian University of
Science and Technology

NTNU

Norwegian University of
Science and Technology

Experiments on Single Droplet Breakage in Turbulent Flow

Ingeborg Dahl

Chemical Engineering and Biotechnology
Submission date: July 2019
Supervisor: Hugo A. Jakobsen
Co-supervisor: Eirik H. Herø
Nicolas La Forgia

Norwegian University of Science and Technology
Department of Chemical Engineering

Abstract

The aim of this master's thesis is to study single droplet breakage in a two-phase turbulent flow. The study includes multiple steps from performing breakage experiments in the laboratory, getting to know and using a droplet breakage video analysis tool developed in MATLAB and performing statistical analysis of experimental data. The intention of the study is to investigate the properties of the breakage, such as breakage time, breakage probability, breakage frequency, number of daughters and the daughter size distribution of a single droplet breakage. The properties of breakage obtained from the statistical analysis of experimental data will be compared to existing models of droplet breakup.

The experiments were performed in a setup with a pump, pumping water from a reservoir tank through pipes into a vertical channel. Oil droplets were released into the water flow in the vertical channel using a syringe pump. Parts of the vertical channel had turbulence enhancing metal rods on the walls to provoke breakage of the oil drops. The droplet breakages were studied through high-speed imaging, shooting at a frame rate of 4000 frames per second. Videos of the droplet breakages were studied and processed in MATLAB. A statistical analysis of the results from the breakages was performed and the results were compared with existing literature.

Two definitions of droplet breakage are considered. The breakage times, t_B for mother droplets of a diameter of 1.10 mm, 1.49 mm and 1.88 mm were found to be 0.0225 ms, 0.0286 ms, and 0.0485 ms respectively using the initial breakage definition. The breakage times found with the cascade breakage definition were 45%, 37% and 72% larger than the initial breakage time definition. Breakages occurring closer to the channel wall were found to have a shorter breakage time, than in the center of the channel. The breakage probabilities, p_B were calculated to be 0.236, 0.341 and 0.345 for droplets with a diameter of 1.10 mm, 1.49 mm and 1.88 mm. The breakage frequencies, b, were estimated using existing models to be 10.5 s^{-1}, 11.9 s^{-1} and 7.11 s^{-1}.

Using the initial breakage definition, all the observed breakages were binary. Using the cascade breakage definition, the number of daughters had a large error due to the size of the data set and the daughter size distribution had a larger error due to the image analysis.

Sammendrag

Hensikten bak denne masteroppgaven er å studere oppbrytningen av enkeltdråper i en turbulent strømning. Oppgave tar for seg flere steg i studien av oppbryting av dråper, inkludert utførelse av eksperimenter på lab, bruk av et analyseverktøy i MATLAB i studiet av dråpeoppbrytningen, samt utførelse av en statistisk analyse av dataene. Formålet med prosjekter er å undersøke egenskaper ved oppbrytning slik som oppbrytningstid, sannsynlighet for oppbrytning, oppbrytningsfrekvens, antall døtre samt størrelsesfordeling på døtre. Disse egenskapene ble sammenliknet med eksisterende litteratur som omhandler oppbrytning av dråper.

Eksperimentene ble utført i et oppsett med en pumpe som pumper vann fra en stor tank inn i en vertikal kanal. Oljedråper ble injisert inn i den kontinuerlige vannfasen ved hjelp av en sprøyte og en pumpe. Deler av den vertikale kanal har metalstaver festet langs to av veggene, som skulle sørge for en mer turbulent strømning og dermed framprovosere oppbrytning av oljedråpene. Oppbrytning av dråper ble studert gjennom høyhastighetskamera som filmet med en hastighet på 4000 bilder i sekundet. Videoer av oppbrytning ble studert og prosessert i MATLAB. En statistisk analyse av resultatene ble utført og sammenliknet med eksisterende litteratur.

To ulike definisjoner for oppbrytning av dråper ble benyttet. Oppbrytningstiden, t_B for mordråper med diametere på 1.10 mm, 1.49 mm og 1.88 mm ble funnet til å være henholdsvis 0.0225 ms, 0.0286 ms and 0.0485 ms ved hjelp av en definisjon som antar at enhver oppbrytning er uavhengig hendelse, 'initial breakage definition'. Oppbrytningstid for dråper med kaskadeoppbrytningsdefinisjonen var 45%, 37% og 72% lengre enn oppbrytningstiden som ble funnet med 'initial breakage' definisjonen. Oppbrytning som oppsto nære veggene i kanalen hadde en kortere oppbrytningstid, enn de som oppsto midt i kanalen. Sannsynligheten for oppbrytning, p_B ble beregnet til å være 0.236, 0.341 og 0.345. Oppbrytningsfrekvensen, b, ble estimert ved hjelp av allerede eksisterende modeller til å være 10.5 s^{-1}, 11.9 s^{-1} og 7.11 s^{-1}.

Ved å benytte seg av 'initial breakage' definisjonen, ble alle de observerte oppbrytningene av mordråper tolket til å være binære. For en kaskadeoppbrytning, inkluderte estimatet for antall datterdråper en usikkerhet som følge av et for lite datasett. Datterstørrelsefordelingen hadde en stor usikkerhet som følge bildeanalysen.

Preface

This master's thesis is submitted as a conclusion of a 5 year study programme, Industrial Chemistry and Biotechnology at NTNU, in the spring of 2019. The last three years were spent in the Chemical Engineering Department. This work is a continuation of a specialization project carried out in the fall of 2018 within the group of Environmental Engineering and Reactor Technology.

I would like to extend my sincere thanks to my supervisor, Professor Hugo A. Jakobsen for your guidance and invaluable insight throughout the process of working with this thesis.

Additionally, I want to express my gratitude to Eirik H. Herø for guiding me through all the steps of this work, for always being available for any questions, for helpful guidance in the performance of the experiments and for fruitful discussions.

A very special thanks to Nicolas La Forgia for providing me with the necessary software for the calibration, the image processing and the statistical analysis as well as helpful advice and insightful suggestions.

I am very grateful to my classmates and for our daily lunch breaks, laughs and motivational conversations. Finally, I would like to thank Olav, for your patience.

Declaration of Compliance

I declare that this is an independent work according to the exam regulations of the Norwegian University of Science and Technology (NTNU).

Trondheim, July 5, 2019

Ingeborg Dahl

Table of Contents

List of Symbols

Latin letters

B_B	$[m^{-3}m^{-1}s^{-1}]$	term in PBE, birth due to breakage
B_D	$[m^{-3}m^{-1}s^{-1}]$	term in PBE, death due to breakage
b_B	$[s^{-1}]$	breakage frequency
C_B	$[m^{-3}m^{-1}s^{-1}]$	term in PBE, birth due to coalescence
C_D	$[m^{-3}m^{-1}s^{-1}]$	term in PBE, death due to coalescence
D	[m]	droplet diameter
f_n	[-]	number density function
n	[-]	number of daughter drops
P_b	[-]	breakage probability
P_D	$[m^{-1}]$	daughter size distribution function
r	[m]	space coordinate
t	[s]	time
t_b	[s]	breakage time
v_D	$[m\ s^{-1}]$	growth rate of particle diameter
We	[-]	Weber number

Greek letters

ε	$[m^2\ s^{-3}]$	turbulent kinetic energy dissipation
μ	[mPa s]	dynamic viscosity
ν	[-]	average number of daughters
ρ	$[kg\ m^{-3}]$	density
σ_I	$[mN\ m^{-1}]$	interfacial tension

Abbreviations

BO	breakage oscillation
CB	cascade breakage
CFD	computional fluid dynamics
fps	frames per second
MO	main oscillation
IB	initial breakage
LDV	laser doppler velocimetry
PBE	population balance equation
pdf	probability density function
TS	threshold

1 Introduction

Turbulent flow is applied in many industrial processes today. This includes operations within the chemical, food, petroleum and pharmaceutical industries. Common for many processes operated at turbulent conditions, is the importance of a high mass and heat transfer in multiphase systems. This may include liquid-liquid separation of a dispersed two-phase flow of two immiscible components, e.g. oil-in-water or water-in-oil dispersions.

The breakup and coalescence of drops and bubbles are of particular interest in dispersed two-phase flows, due to the fact that breakup and coalescence have a direct influence on the interfacial area between the continuous and dispersed phases [1]. The interfacial area will affect the transfer of mass and heat between the phases.

Droplet breakup in a turbulent flow is traditionally considered to be caused by turbulent stresses along the surface of the drops [2]. These turbulent stresses are caused by collisions with turbulent eddies and cause the particles to deform. When the deformation of the particle has resulted in a sufficient stretch of the shape of the particle, the particle is fragmented into smaller daughter particles. Viscous stresses may cause a velocity gradient that leads to a particle deformation and eventually breakage. However, these viscous stresses are often neglected for turbulent flows, which is a good assumption for lower pressures. A simple illustration of a drop breakup is illustrated in Figure 1.1. The initial droplet is frequently referred to as the *mother* drop. After a breakup, the final distribution consists of two or multiple *daughter* drops, all originating from the original mother drop.

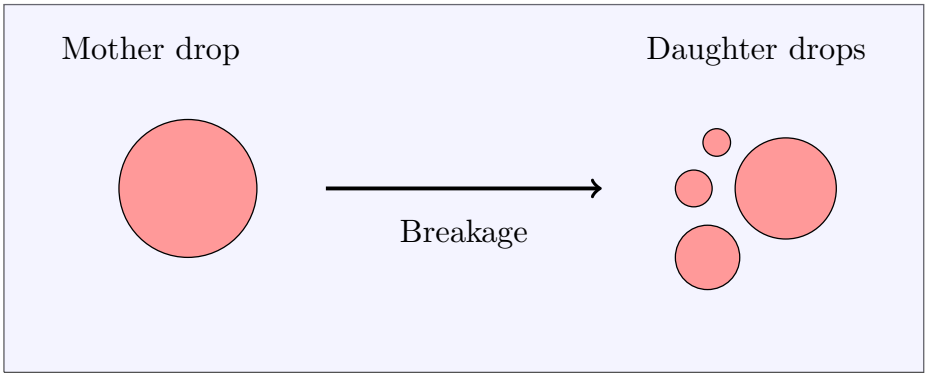

Figure 1.1: A simple illustration of a droplet breakage. The mother droplet is the initial droplet that breaks into two or more daughter drops.

Owing to the fact that dispersed two-phase flows play such an important role in so many industrial processes today, it is essential to gain knowledge about the mechanisms behind the behavior of such systems. This includes gaining extensive knowledge of the breakup events of dispersed two-phase flows.

It is rather difficult to formulate generalized models for particle breakage and coalescence using basic hydrodynamics and physical properties [3]. Population balances can be used to describe the changes in the fluid particle size distribution. A disadvantage of the population balance is the requirement of models for the breakage and coalescence. Solsvik et al. [2, 4] investigated numerous models used for particle breakage and concluded that in order to improve the existing models, extensive, well-planned, model-based experiments are needed. Further investigations were particularly needed for single particle experiments seeking to find models for breakage frequency, number of daughters and daughter size distribution functions. In this work, the breakage of single drops has been thoroughly investigated in order to verify existing models.

2 Theory

2.1 The Population Balance Equation

A population balance is a useful modeling tool, first presented as a concept by Hulburt and Katz [5]. The concepts have been adopted to investigate various populations, such as biological systems (Ramkrishna [6]) and liquid-liquid dispersions (Coulaloglou and Tavlarides [3], Lou [7] and Luo and Svendsen [8]). The population balance equation describes the temporal variation [9] of the fluid particle distribution due to the advection, growth, coalescence and breakage processes [10]. This is done by keeping record of the number of dispersed entities in a dispersed system [11]. The equation is written in the form of a number density function, f_{n}, and contains information of how the size, shape, temperature and position of the entities are distributed in space and time. The equation can be given as [11]

$$\frac{\partial f_n(D,\mathbf{r},t)}{\partial t} + \nabla_r \cdot [\mathbf{v_r}(D,\mathbf{r},t) f_n(D,\mathbf{r},t)] + \nabla_D \cdot [v_D(D,\mathbf{r},t) f_n(D,\mathbf{r},t)] \quad (1)$$

$$= -B_D(D,\mathbf{r},t) + B_B(D,\mathbf{r},t) - C_D(D,\mathbf{r},t) + C_B(D,\mathbf{r},t)\left[\frac{1}{\mathrm{sm}^3}\right],$$

where t is the time coordinate and $\mathbf{r}$ is the space coordinate, D is the fluid particle diameter. Furthermore, $\mathbf{v_r}$ is the velocity in physical space and v_{D} is the growth rate of the particle diameter. The right hand side of the equation describes how break-up and coalescence, B and C result in deaths and births in the particle population respectively, subscripted D and B.

This research project seeks to explain the break-up of the droplet, thus, the coalescence is not of importance. The death and birth of the fluid particles as a result of droplet breakage, can be given as [11].

$$B_D(D,\mathbf{r},t) = b_B(D) f_n(D,\mathbf{r},t) \quad (2)$$

$$B_B(D,\mathbf{r},t) = \int_D^{D_{max}} \nu P_D(D,D') b_B(D') f_n(D',\mathbf{r},t) \mathrm{d}D' \quad (3)$$

Here, b_B is the breakup frequency, ν represents the number of daughter droplets generated and P_D is the daughter size distribution probability density function. P_D can be described using different models [2], among them are (i) empirical, (ii) statistical and (iii) phenomenological models. Empirical models are less frequently used, at they are valid for only a limited range of applications. Statistical models include known probability distribution functions for random variables

such as a discrete, Gaussian, β and random distribution. Phenomenological models use simple relationships to relate empirical observations of presumable important phenomena to each other.

2.2 Models for the Breakage Frequency b_B

Numerous models for the breakage frequency has been suggested. These models have included binary breakage in the interial subrange (Han et al. [12]), multiple breakage in the intertial subrange (Han et al. [13]) and multiple breakage in the wide energy spectrum (Han et al. [14]). Two models of particular importance for the breakage frequency are presented below.

2.2.1 Coulaloglou and Tavlarides (1977)

Coulaloglou and Tavlarides [3] proposed models to describe droplet breakage and coalescence in a turbulent liquid-liquid dispersion and concluded that the models could be used for predictions of properties such as drop size distribution.

They defined the breakage frequency, $b_B(D)$, as

$$b_B(D) = \frac{1}{t_b(D)} \frac{\Delta N(D)}{N(D)} \tag{4}$$

where $t_b(D)$ is the breakage time and $\frac{\Delta N(D)}{N(D)}$ is the fraction of droplets breaking. $\frac{\Delta N(D)}{N(D)}$ is found by approximating it to be proportional to the fraction of turbulent eddies colliding with the droplet.

$$\frac{\Delta N(D)}{N(D)} = \exp - \frac{c_1 \sigma_I}{\rho_d \epsilon^{2/3} D^{5/3}} \tag{5}$$

where c_i are system specific constants for $i \in \{1, 2, 3\}$ used in the models by Coulaloglou and Tavlarides, σ_I is the interfacial tension, ρ_d is the density of the disperse phase and ϵ is the turbulent kinetic energy dissipation. The breakage time was approximated using an assumption that the centre of mass for the two daughter droplets move similarly to the relative motion of two turbulent eddies.

$$t_b(D) = c_2 D^{2/3} \epsilon^{-1/3} \tag{6}$$

By combining the results from Equation 4, Equation 5 and Equation 6, the obtained equation for the breakage frequency is given as

$$b(D) = c_3 D^{-2/3} \epsilon^{1/3} \exp - \frac{c_1 \sigma_I}{\rho_d \epsilon^{2/3} D^{5/3}} \tag{7}$$

2.2.2 Martínez-Bazán et al. (1999)

Martínez-Bazán et al. [15, 16] proposed a model that restricts itself to homogeneous and isotropic turbulent flows, but avoids the concept of turbulent eddies.

With the assumption of binary breakup and negligible viscous effects, the model is similar to the model of Coulaloglou and Tavlarides.

The basic premise for the model is that for a bubble to break, the surface has to deform. The deformation energy required is supplied by turbulent stresses and has to be larger than the surface energy. Martínez-Bazán et al. defined the breakage frequency as

$$b_B(\epsilon, D) = \frac{1}{t_B(D)}, \tag{8}$$

meaning the breakage frequency is inversely proportional the bubble breakup time, $t_b(D)$. The bubble breakage time estimation is

$$t_b \propto \frac{D}{\sqrt{\overline{\Delta \mathrm{v}^2(\mathrm{D})} - 12\frac{\sigma_I}{\rho_c D}}} \tag{9}$$

where the mean value of the velocity fluctuations, $\overline{\Delta \mathrm{v}^2(\mathrm{D})}$, is estimated to $\beta(\epsilon D)^{2/3}$, following Kolmogorov's universal theory for homogeneous and isotropic fluids. ϵ is the turbulent kinetic energy dissipation, σ_I is the interfacial tension and ρ_c is the density of the continuous phase. Thus, the expression for the breakage frequency is given as:

$$b_B(\epsilon, D) = K_g \frac{\sqrt{\beta(\epsilon D)^{2/3} - 12\frac{\sigma_I}{\rho_c D}}}{D} \tag{10}$$

With a critical diameter, D_C, of

$$D_C = \left(\frac{12\sigma}{\beta\rho_c}\right)^{3/5} \epsilon^{-2/5} \tag{11}$$

Droplets with a diameter $D < D_C$ will have a breakage frequency of zero.

This model is developed for flows with a high Reynolds number and assumes that all drops break. Solsvik et al. [17] studied the model and proposed to extend the breakage frequency model by Martínez-Bazán to include droplet breakage probability. The extention of the model was inspired by the model of Coulaloglou and Tavlarides (see section 2.2). The breakage probability was defined as [17]

$$P_b = \frac{\Delta N(D)}{N(D)} = \begin{cases} 0 & \text{if } d < d_{crit} \\ \exp\frac{E_{crit}(d-d_{crit})}{E(d-d_{crit})} & \text{if } d > d_{crit} \end{cases} \tag{12}$$

2.3 Previous work on single drop breakage in turbulent flow

2.3.1 Pilch and Erdman (1987)

Pitch and Erdman [18] used the Weber number to characterize breakage properties. The Weber number is a dimensionless property used for analyzing fluid flows with an interface between the phases. An interfacial shear Weber number was defined:

$$We_{int,shear} = \frac{\text{interfacial shear stresses}}{\text{surface tension stresses}} \tag{13}$$

A $We_{int,shear}$ less than or equal to 12 indicates that the turbulent breakage happens due to oscillations that eventually break the droplet into two of more fragments.

2.3.2 Galinat et al. (2005,2007)

Galinat et al. performed particle breakage in an orifice pipe flow [19, 20]. The breakages were studied in a high speed with a record rate of 500 fps. The number of daughters and the size of the daughters were studied as a function of the Weber number. The number of daughters were found to be an increasing function of the Weber number, whereas the daughter drop size was found to be decreasing with the Weber number. At low Weber numbers, the daughter distribution exhibited a multi-modal shape, which is characteristic for daughters of unequal drop diameters. At higher Weber numbers, the daughter distribution exhibited a single modal shape. The breakage probability was concluded to be monotonously increasing withe the Weber number.

2.3.3 Andersson and Andersson (2006)

Andersson and Andersson [21] studied bubble and drop breakage in high speed cameras and found that for bubbles, the only outcome was a binary breakage with uneven daughter bubbles due to internal flow redistribution mechanisms. Drops were most probable to go through ternary breakage, most commonly forming equal sized drops, since there are no internal flow redistribution mechanisms due to the much higher viscosity. Figure 2.1 shows the number probability function for drop breakage in a dodecane-water system at two different flow conditions. This is illustrated by plotting the frequency of the number of daughter fragments.

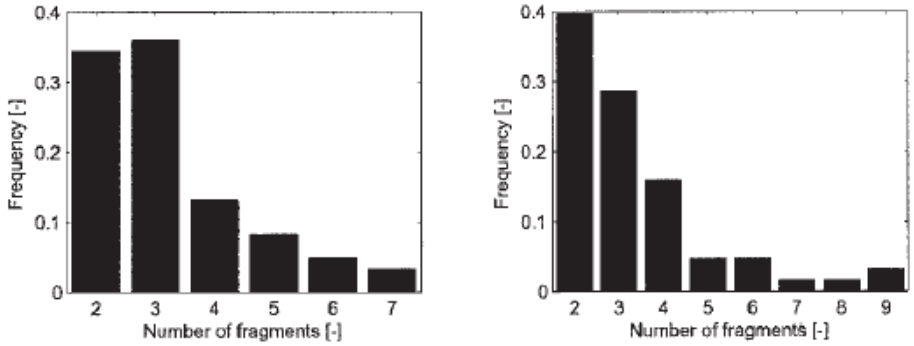

Figure 2.1: Number probability function for drop breakage for a dodecane water system at two different flow conditions [21].

Figure 2.2 shows the daughter droplet size distribution, represented by the volume fraction of the largest fragment of a breakage for bubbles and drops.

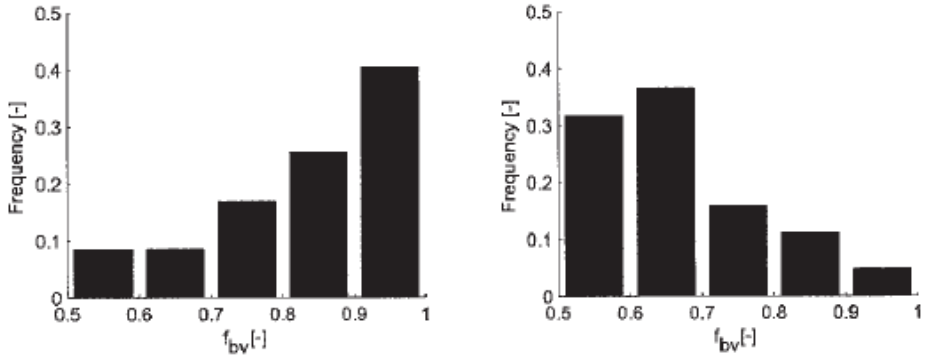

a) Bubbles b) Drops

Figure 2.2: Volume fraction of the largest fragment for bubbles (a) and drops (b) [21].

Andersson and Andersson [22] proposed a new model based on the observation that the droplets and bubbles were subjects to strong deformation before breakage. The model presented was insensitive to the size of the turbulent structures hitting the droplets, and formulated in terms of interaction frequencies. Vali-

dation of this model with experimental measurements gave better results than traditional models.

2.3.4 Maaß et al. (2007) and Zaccone et al. (2007)

Maaß et al. [9, 23] looked at single drop breakage in stirred liquid-liquid systems using an optical measurement technique with a record rate of 650 frames per second. A mathematical model for the daughter drop size was developed. The empirical model suggested that for smaller drops, the most frequent outcome of the initial breakage was a binary breakage, whereas for larger drops, the most common was a ternary breakage. Figure 2.3 shows the probability of the number of daughter droplets, ν, generated by a droplet breakage at a velocity of 1 ms^{-1}.

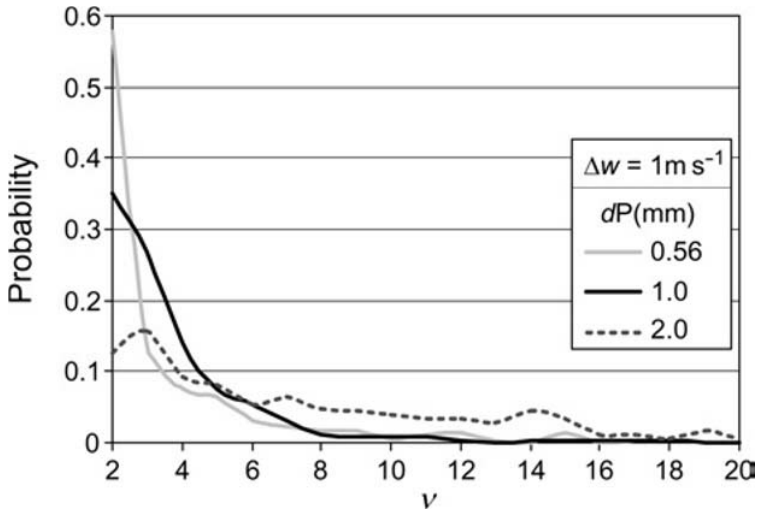

Figure 2.3: Probability of number of daughter drops, ν with varying mother drop diameter, d_p, for a velocity of 1ms^{-1} found by Maaß et al. [23].

Figure 2.4 shows how the velocity affects the probability of the number of daughter droplets generated for a 1 mm droplet in the experiments performed by Maaß et al.

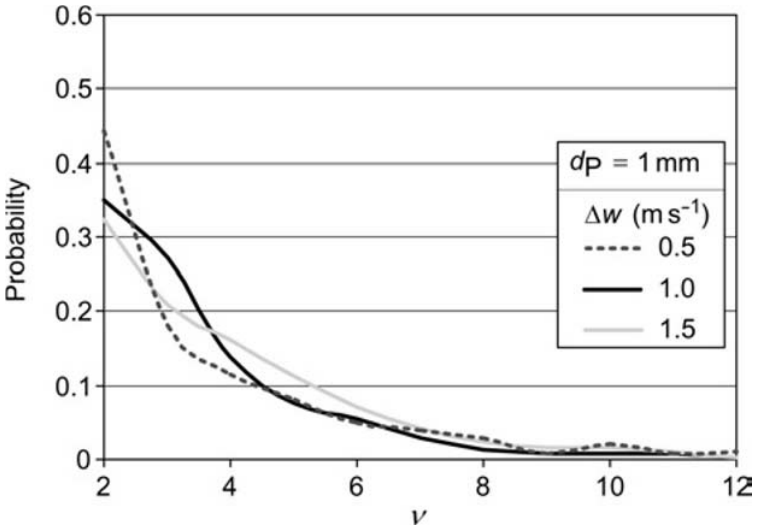

Figure 2.4: Probability of number of daughter drops with varying flow velocity, Δw, for a drop with a diameter, d_P, of 1mm found by Maaß et al. [23].

Zaccone et al. [24] presented a daughter droplet size probability density function, pdf, based on a mathematical pdf by Diemer and Olsson [25].

2.3.5 Maaß et al. (2009)

It is commonly known that turbulent flow breakage is closely related to the energy dissipation rate. Maaß et al. [26] investigated particle strain and breakup in an experimental setup with a stirred vessel. Computational fluid dynamic investigations, CFD, was performed to investigate the flow pattern in the vessel. The results of the CFD showed that the area where breakage occurred, behind the stirrer blade, had the highest energy dissipation rates.

2.3.6 Maaß and Kraume (2012)

Experimental testing from Maaß and Kraume [27] showed that the smaller parent particle sizes gave the highest breakage frequency for petroleum-systems and toluene-water system.

2.3.7 Nachtigall et al. (2016)

Nachtigall et al. [28] analyzed drop deformation dynamics in a turbulent flow using MATLAB and statistical analysis to automate the process. The experiments were performed in the same setup as Maaß and Kraume [27]. Different deformation parameters were discussed to describe the oscillations before breakage. The highly deformed droplets were described using a perimeter ratio, using the relation between the perimeter of the particle and the perimeter of an area equivalent circle.

2.3.8 Solsvik and Jakobsen (2015)

Solsvik and Jakobsen [29] performed single drop experiments in a stirred liquid tank for different oils. Their results suggested that multiple breakup events were the most common and that the number of daughters depended on the mother droplet size. Increasing droplet size resulted in a decreasing probability of a binary breakage. Figure 2.5 shows the probability of binary and multiple breakage for toluene, 1-octanol, petroleum and n-dodecane.

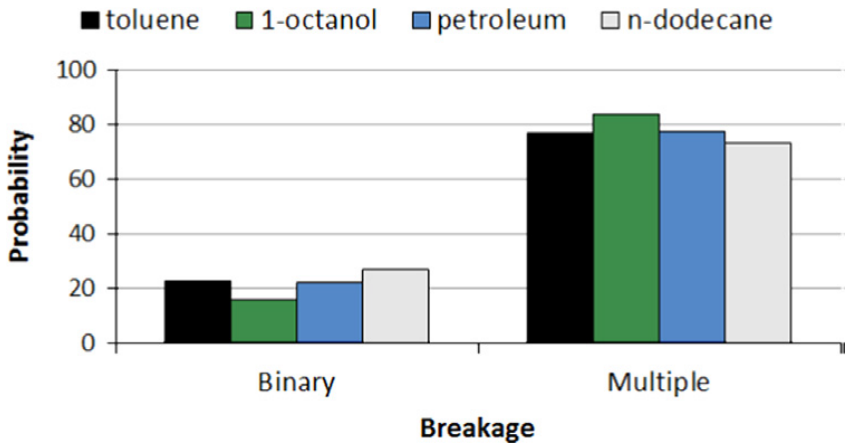

Figure 2.5: Probability of binary and multiple breakage for the different types of oils in Solsvik's experiments [29].

Figure 2.6 shows how the breakage time changes with the mother droplet diameter for different types of oil. The trend from these experiments, is an increasing breakage time with an increasing mother droplet time.

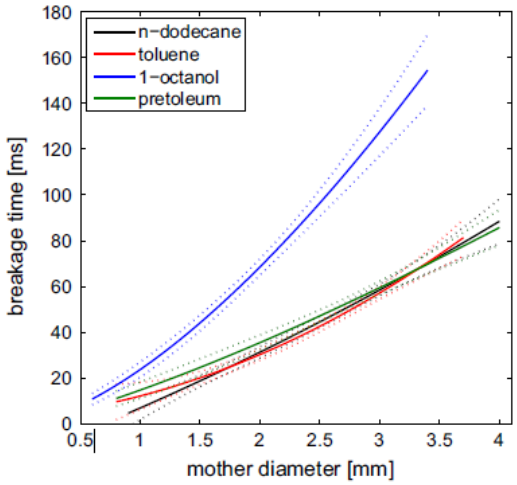

Figure 2.6: Breakage time plotted as a function of mother drop diameter for the different oils in Solsvik's experiments [29].

Figure 2.7 displays the probability for the number of daughter droplets in a final distribution for the different oils.

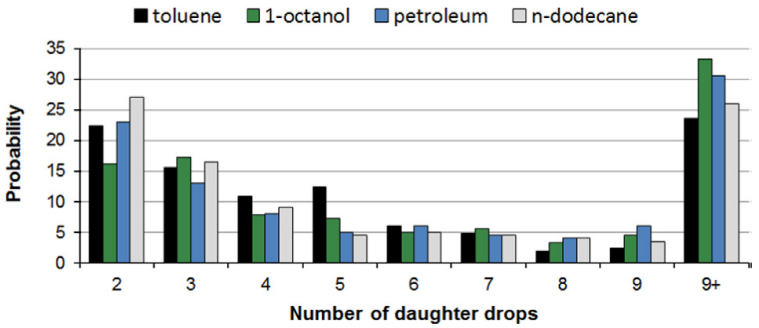

Figure 2.7: Probability for the number of daughter droplets generated in a breakage in Solsvik's experiments [29].

2.3.9 Solsvik and Jakobsen (2016)

Solsvik and Jakobsen [11] studied the breakage of droplets in turbulent flow using high speed imaging. Two different definitions were suggested for the droplet break-up event. The two definitions are illustrated in Figure 2.8, both considering an initially stable droplet with a spherical shape. Energy for the break-up can be obtained from a collision with a turbulent eddy, causing the mother droplet to start deforming.

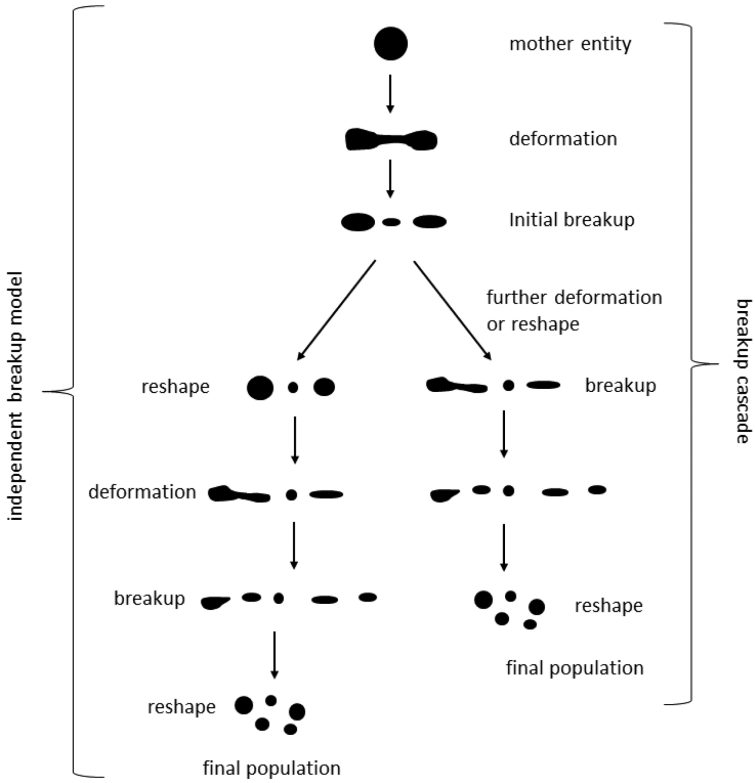

Figure 2.8: Illustration of initial breakup, a breakup cascade and an independent breakup model [11].

The initial breakup definition includes the first observed breakage into new daughter droplets. Any further deformation and breakage is considered to be a part of a new breakup event. Using this definition, each new breakage is considered to be an independent event. Their conclusion was that binary breakup was a fair assumption if only the initial breakup was studied. They also concluded

that the usage of the historically used initial breakage definition could cause erroneous estimates of the droplet breakage rate.

The cascade definition of a breakage considers a breakup event consisting of a sequence of breakups from til initial breakup until the daughter drops stabilizes do not undergo any more breakups. Any droplets formed during a cascade breakage is considered an intermediate daughter until the droplets do not undergo any deformation anymore.

3 Statistical Analysis

Statistical analysis of the data is of great importance, due to the large labor of image analysis. The error of the estimates of the breakage time, number of daughters, breakage probability and breakage breakage frequency are necessary to know, in order to know if the dataset is sufficiently large enough. The statistical distributions are found in Wheeler and Ganji [30] or Box et al. [31].

Standard Normal Distribution/Gaussian Distribution

The expectation value, μ, for parameters such as breakage time and number of daughters are approximated by an average value, $\hat{x}$. Average values can be assumed to have a Gaussian distribution with a standard deviation σ. Average values can be assumed to have a normal distribution, with a confidence interval of

$$\mu = \hat{x} \pm z_{\alpha/2} \frac{\sigma}{\sqrt{n}} \quad \text{for a confidence level 1 - } \alpha \tag{14}$$

where $z_{\alpha/2}$ is the upper critical value for the standard normal distribution for a confidence level of 1 - α and can be found in statistical tables [32].

Binomial Distribution

The breakage probability is assumed to have a binomial distribution. The binomial distribution describes a random, discrete variable with the only two outcomes, 'success' and 'failure'. An experiment with a binomial distribution assumes a constant probability of success, P. For droplet breakage experiments, P denotes the breakage probability. A binomial experiment assumes n number of independent trials. The binomial distribution, $P(r)$, provides information about the probability that r trials out of n are successful. The distribution is expressed below in Equation 15.

$$P(r) = \binom{n}{r} p^r (1-p)^{n-r} \tag{15}$$

The expected numbed of successful trials in n trials can be expressed as

$$\mu = np \tag{16}$$

The standard deviation of the binomial distribution is

$$\sigma = \sqrt{np(1-p)} \tag{17}$$

4 Experimental

4.1 Experimental Setup

4.1.1 Apparatus Overview

A schematic illustration of the experimental setup is presented in Figure 4.1 [33]. The experimental setup consists of a closed circuit connected by pipes with a continuous phase of de-ionized water running through the circuit.

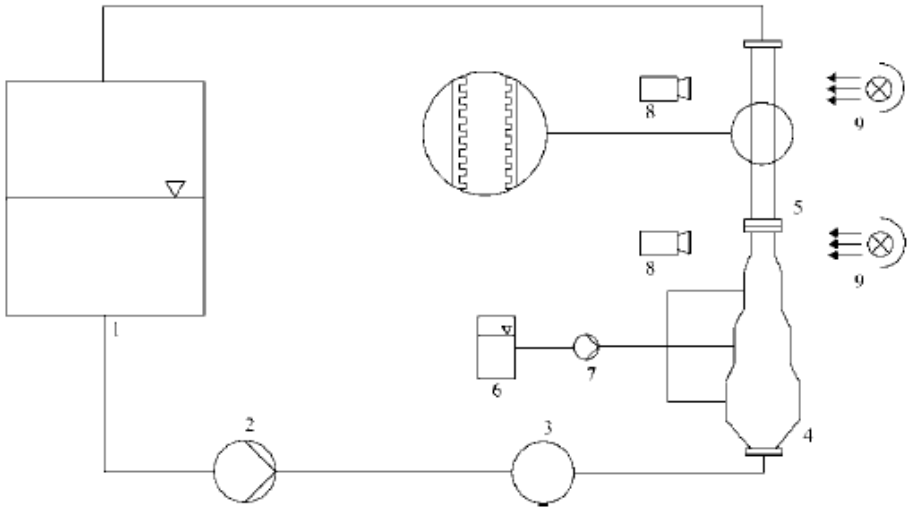

Figure 4.1: Schematic illustration of the setup [33]. 1. Water tank, 2. Pump, 3. Flow meter, 4. Droplet Generation Channel, 5. Breakage channel, 6. Oil tank, 7. Oil pump, 8. Camera, 9. Lights

A large water reservoir tank (1) supplies a mechanical pump (2) of the type *MDL-0670* from *SPX Flow Technology* with the de-ionized water, pumping the water flow through a flow meter (3) into a vertical channel (4), hereby entitled the droplet generation channel. A needle is used for generating droplets. This needle can be placed at three different heights into a part of the channel, hereby denoted at the droplet generation channel. The droplet generation channel has a square cross-section and the cross-sectional area is decreasing with the height of the channel. Oil is supplied to the needle from a syringe (6) through a pipe using a pump (7) controlled in software developed using *LabView*. Usage of the software for administrating the experiments will be explained in section 4.1.10.

From the droplet generation channel, the continuous water phase and the dispersed oil drops flows into a part of the channel with a smaller cross-sectional area, entitled the breakage channel (5). Two of the breakage channel walls are covered with periodical metal rods to enhance turbulent flow and provoke droplet breakage. The breakage channel is under surveillance by two high speed cameras (8) and illuminated up by lights (9). From the breakage channel, the water flows back into the water tank (1).

4.1.2 Mechanical Pump

The mechanical pump, shown in Figure 4.2a, is used to pump the water from the water reservoir tank through the circuit. It is an MDL-0670 from SPX Flow Technology. Figure 4.2b displays the setup for the pump control panel.

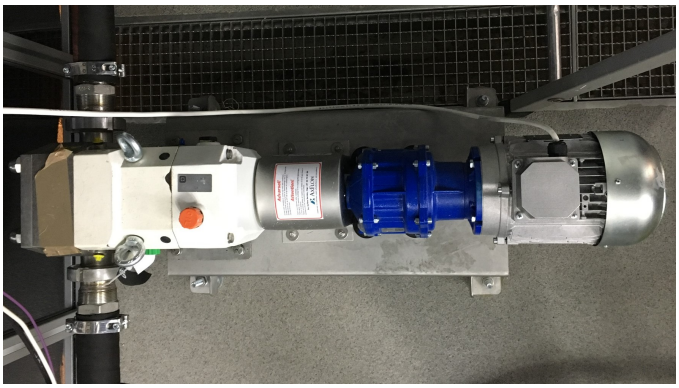

(a) Mechanical pump

(b) Control panel for the pump

(c) The pump is switched on and off by pressing the green and red button respectively.

Figure 4.2

The electrical supply to the mechanical pump is turned on and off by pressing the green and red button shown in Figure 4.2c. The mechanical pump is controlled from a control panel from ABB, seen in Figure 4.3. Pressing the 'START' and 'STOP' turns the pump on and off. An LCD screen displays essential pump settings. The pump frequency is adjustable and is displayed in the centre of the screen. The bottom left corner reveals whether the control panel is operating at input or output mode. Output mode is applied for the mechanical pump. The bottom right corner indicates the direction of the motor, and thereby also the direction of the water flow, and displays 'FWD' if the motor is running forward and 'REV' if the motor is running in reverse. The direction can be changed by pressing the 'DIRECTION' button.

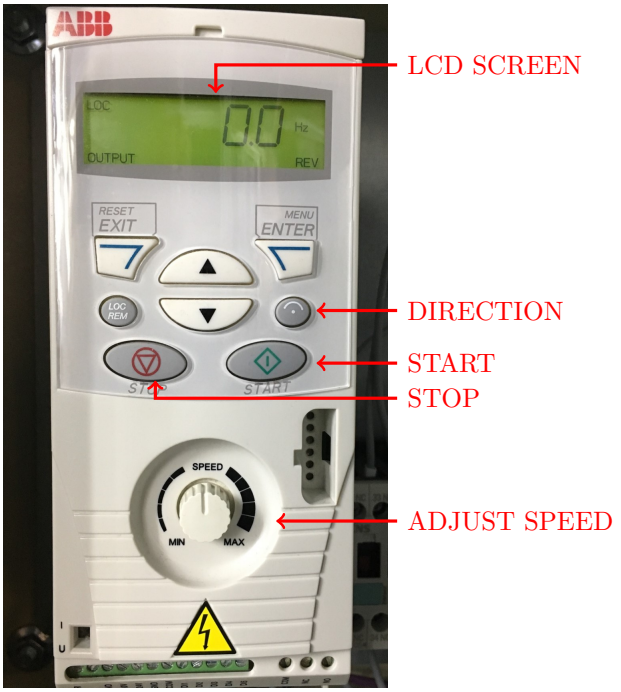

Figure 4.3: Control panel for the mechanical pump.

4.1.3 Flow Meter

The flow meter is a SITRANS F M MAG 5000 from Siemens and is shown in Figure 4.4. It is connected to the pipeline after the pump and measures the flow rate of the continuous phase. The signal from the flow meter is connected to a computer and the software for controlling the experiments with an acquisition card.

Figure 4.4: Flow meter from Siemens

4.1.4 Droplet Generation Channel

Figure 4.5 is a collage of images of the droplet generation section. There are 3 different inlets at different heights, and with different cross-sectional areas. A needle, used for droplet generation, is positioned in either of the three inlets. The needle is supplied with oil through a pipe connected to the syringe pump.

Figure 4.5: Section for droplet generation from different angles.

4.1.5 Syringe Pump

Figure 4.6 shows the syringe pump from KD Scientific. The syringe is secured onto the pump by retaining brackets and a clamp fastened to the barrel. A pusher block moves the plunger forward, pushing the oil into the pipe, which is connected to the droplet generating needle. An LCD screen can be used for monitoring and controlling the syringe, but this can also be done from the software for controlling the experiments. The acquisition card connects the syringe pump and the computer software.

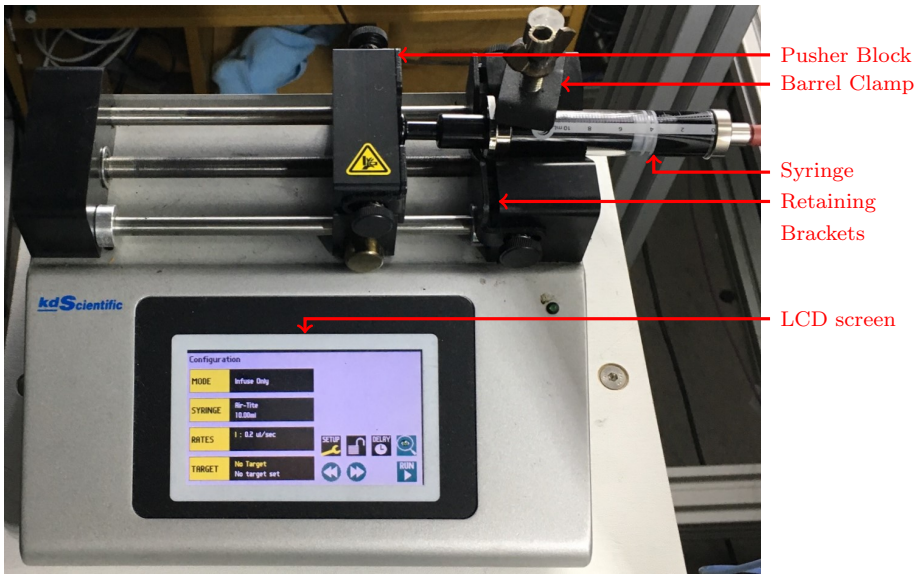

Figure 4.6: Syringe pump

4.1.6 Breakage channel

The breakage channel is a 1m long channel with a square, 30mm by 30mm, cross-section. Two opposing walls are made of glass to facilitate the recording of droplet breakup. The other two walls are covered with metal rods to enhance turbulent flow in the channel. The metal rods are 3mm by 3mm by 30mm and placed with a 10mm distance between the centre of the rods. A simple sketch is illustrated in Figure 4.7. Furthermore, a photo of the breakage channel is included in Figure 4.9.

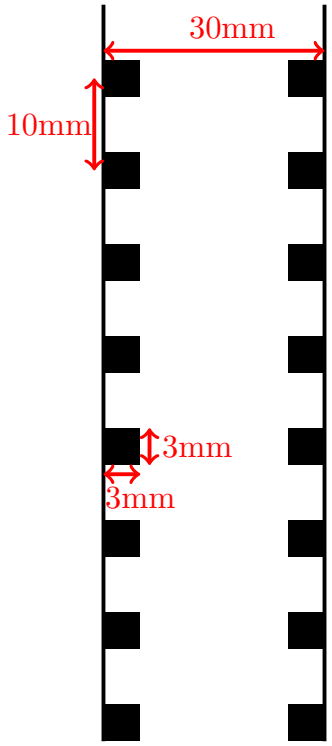

Figure 4.7: Simple sketch of the breakage channel.

4.1.7 Camera

The oil droplets are observed in the breakage channel through high speed cameras. Two Photron FASTCAM Mini AX100 540K M3 cameras are facing the breakage channel. Both are mounted to metal shelves, screwn tight to reduce vibrations. The shelves can be moved up and down, to position the cameras at different heights in relation to the breakage channel. By moving the shelves forward, the image is zoomed in to get a more detailed image. To fit more of the breakage channel in the image, the shelves can be moved backwards to zoom out. The vertical distance between the cameras, and the angle of the cameras on the shelves, ensuring that there is an overlap in the images of the breakage channel from the two cameras. This way, the cameras catch a longer part of the breakage channel on camera. An acquisition card connects the cameras and the computer with the software for controlling the experiments.

Figure 4.8: Camera setup with two Photron FASTCAM Mini AX100 540K M3 cameras mounted to metal shelves.

The cameras can record at a frame rate of 4000 frames per second, which is equivalent to 0.25 ms between each frame. The focus of the camera is manually adjustable by twisting the camera lens.

4.1.8 Lighting

Lighting is a crucial part of the experimental setup, due to the requirement of high quality images of the droplet breakages. The breakage channel is lit through the opposing side relative to the cameras. Three lights are positioned on top of each other. Using sheets of paper, the light is diffused to make sure that the light is soft and evenly distributed across the breakage channel.

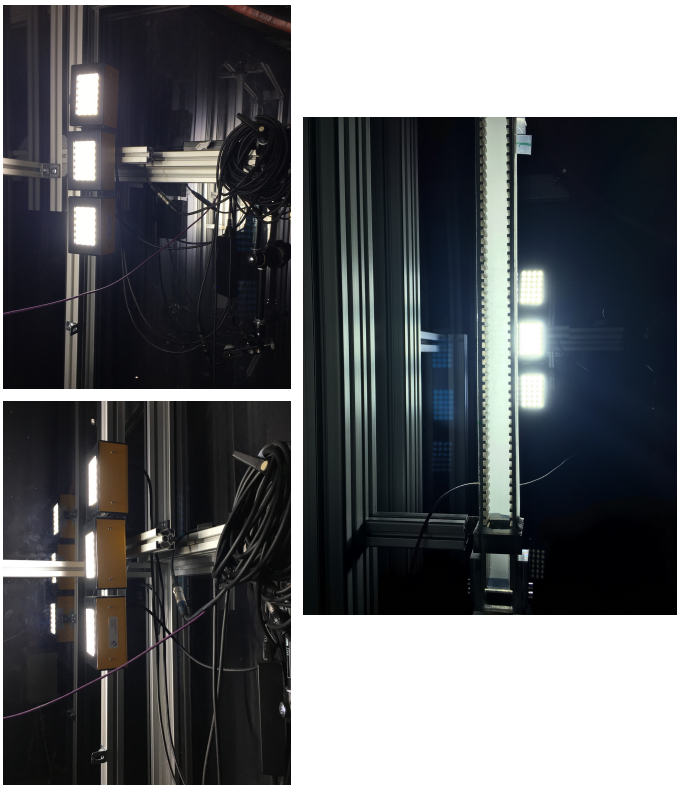

Figure 4.9: Lighting setup. Three lights are placed in a vertical line on top of each other. The lights are directed towards the breakage channel on the opposite side of the channel of the cameras, resulting in the breakage channel being lit up from behind.

4.1.9 Acquisition Card

Figure 4.10 shows the acquisition card from National Instruments. This connects the measurements from the thermometer and the flow meters, the images and camera settings and the syringe settings to the software for controlling and monitoring the experiments.

Figure 4.10: Acquisition card

4.1.10 Software for Controlling and Monitoring the Experiments

Experiments are controlled from a software developed in LabView. This software connects the information from the experimental set-up through the acquisition card. The graphical user interface for the software is shown in Figure 4.11. The important features of the software will go through further elaboration in this section.

The interface includes the camera view from the breakage channel, sections for camera and ROI settings, sections for the syringe pump and the water pump and a section for controlling droplet detection.

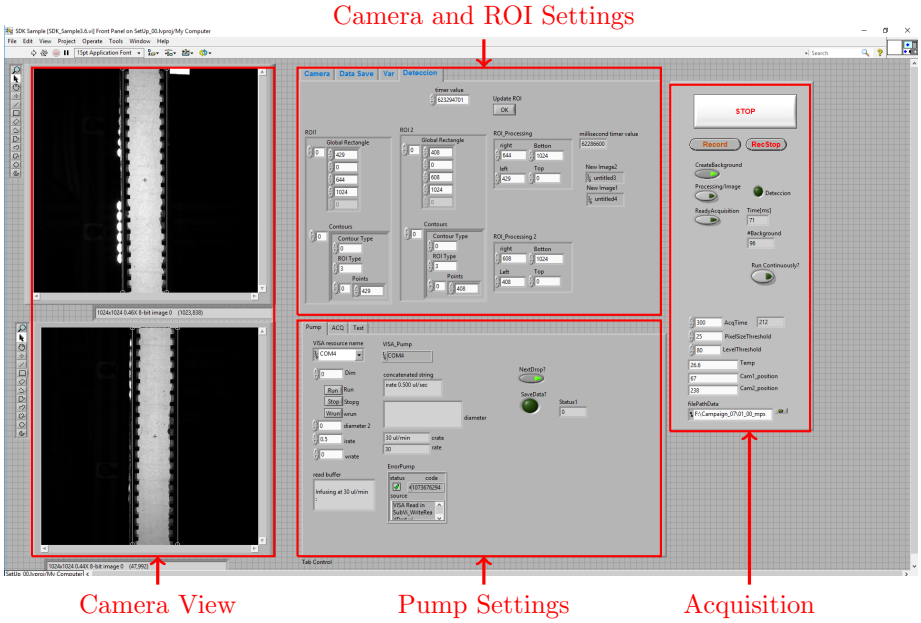

Figure 4.11: Graphical user-interface of the software used during experiments.

Camera settings

The standard camera settings are presented in Figure 4.12. The frame rate or 'Record Rate' (1) indicates the frequency at which the frames are recorded on the camera. Standard frame rate used during the experiments is 4000 fps (frames per second) The 'Resolution' (2) was standardized to 1024 by 1024 pixels. Shading (3) is used to improve the quality of the images while the cameras are in use. The shutter speed (4) refers to length of time the camera sensor is exposed to light. A shutter speed of 1/25000 sec was used during the experiments.

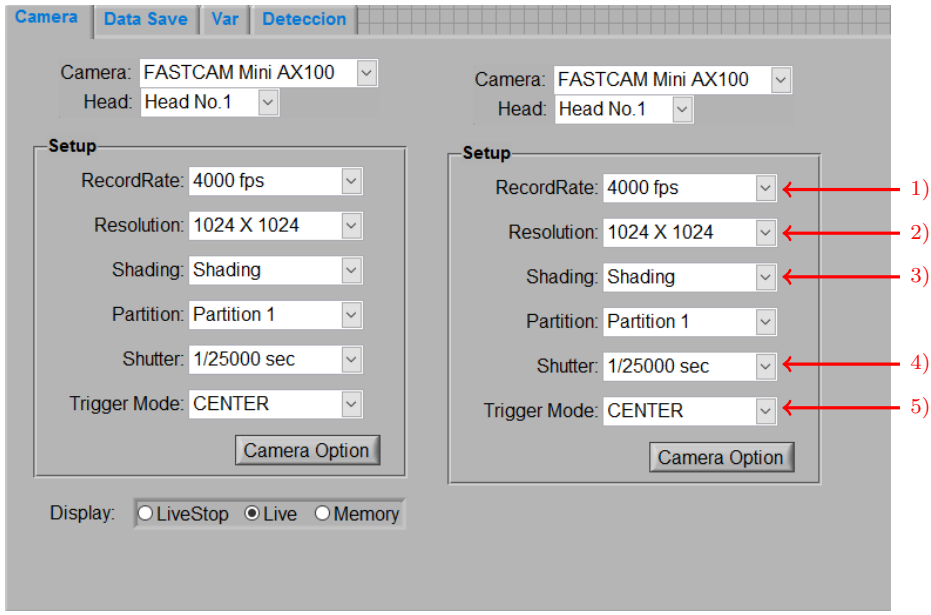

Figure 4.12: User interface for the camera settings.

'Trigger mode' (5) decides how the video footage is saved when something triggers the detection. The possible trigger modes are 'START' and 'CENTER'. The trigger modes are closely related to the term acquisition time.

The acquisition time is related to expected amount of time a droplet will spend in the camera shot and determines the length of the droplet videos. Different velocities of the continuous phase, and thereby also different velocities of the oil droplets, will have different acquisition times. A simple empirical rule is used to find the acquisition time:

$$\text{Acquisition time } [\text{ms}] \simeq \frac{0.17\,[\text{m}]}{u\,[\text{m/s}]} * 1000 + 20\,[\text{ms}],$$

where u is the velocity of the continuous water flow in m/s and 0.17 m is the length of the breakage channel that is visible on the camera. The fraction is multiplied by 1000 to convert from seconds to milliseconds. An extra 20 ms is added to ensure the complete path of the droplet is caught on camera.

Using the trigger mode 'START', the software saves the footage from the moment a droplet is detected. The duration of the footage is 2 times the acquisition time. The trigger mode 'CENTER' saves the images from one times the acquisition time before the detection and two times the acquisition time after the detection. This ensures that if a droplet is detected in the middle of the breakage channel, the entrance of the droplet into the breakage channel is not lost. 'CENTER' was used as the standard trigger mode. A graphical interpretation of the trigger mode is shown in Figure 4.13.

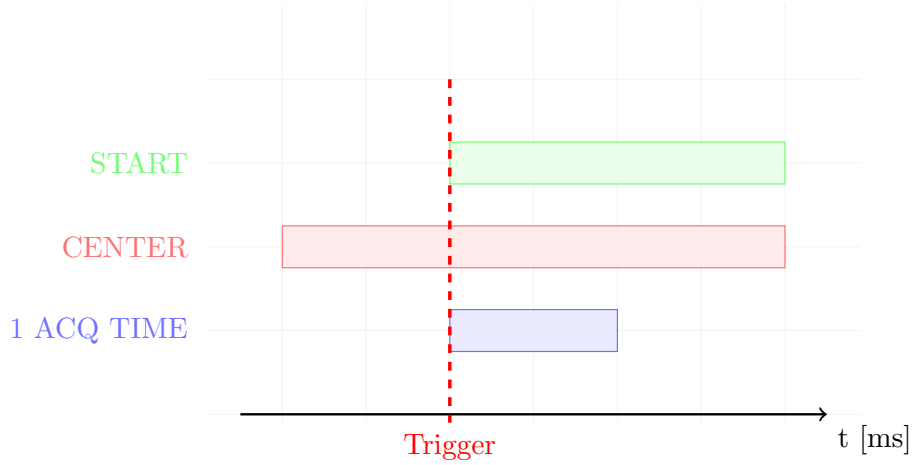

Figure 4.13: Graphical interpretation of how the trigger modes save droplet footage.

ROI

The ROI indicates the area *of interest* of the camera view. When the experiments are running, the software will actively search for droplets within the ROI. Consequently, the area within the ROI should cover the breakage channel, as illustrated in Figure 4.14.

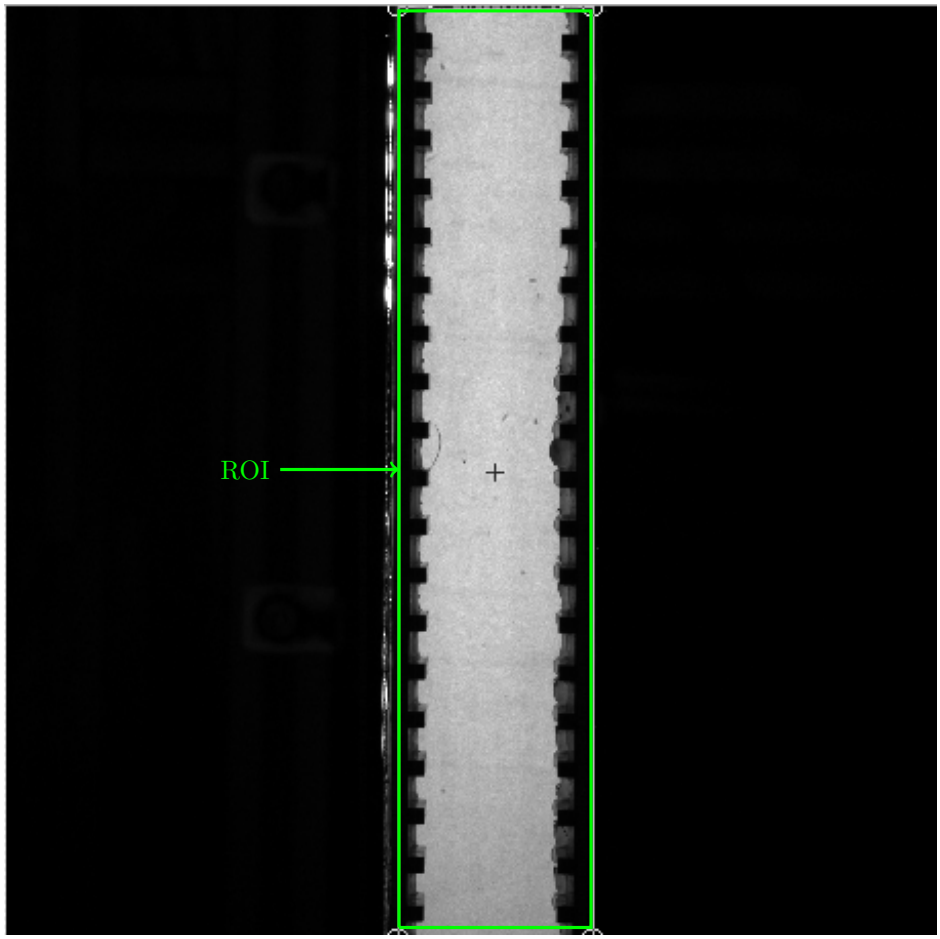

Figure 4.14: Camera view. The ROI is the area marked in green.

Whenever any adjustments are done to the position of the camera, the ROI must be updated. The ROI can either be set by manually writing the pixel coordinates for the outline of the ROI into the user interface presented in Figure 4.15 or by marking the area on the live images from the cameras and clicking 'Update ROI'.

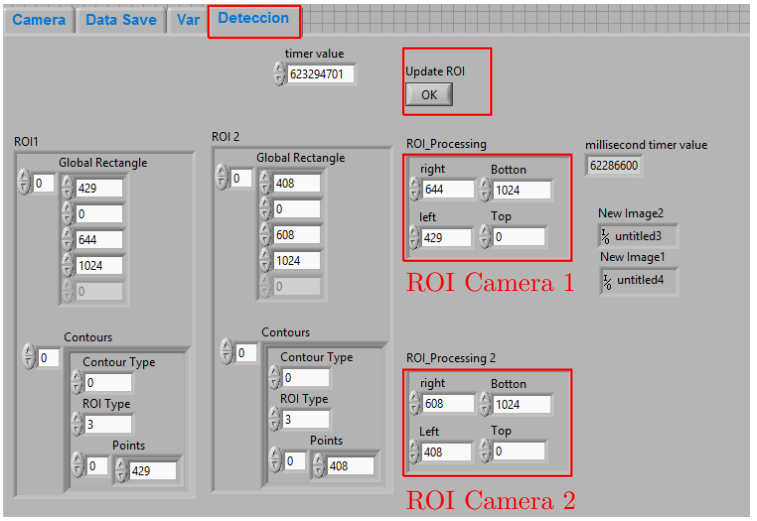

Figure 4.15: Under the tab 'detection' it is possible to adjust the ROI, which is the area of the image that is saved in the detection files. The ROI can be adjusted in the areas marked in red and by clicking on 'Update ROI'.

Control of Syringe Pump

The software used during experiments allows control of the syringe pump. This is done in the tab 'Pump'. A crop of the software in which the control of the pump is carried out, is shown in Figure 4.16. The syringe pump can be started and stopped manually on the control panel on the syringe pump (see section 4.1.5) and by pressing 'Run' (1) and 'Stop' (2). However, the pump will also start pumping oil automatically when starting the droplet detection. This will be explained further in section 4.2.2, Droplet Detection.

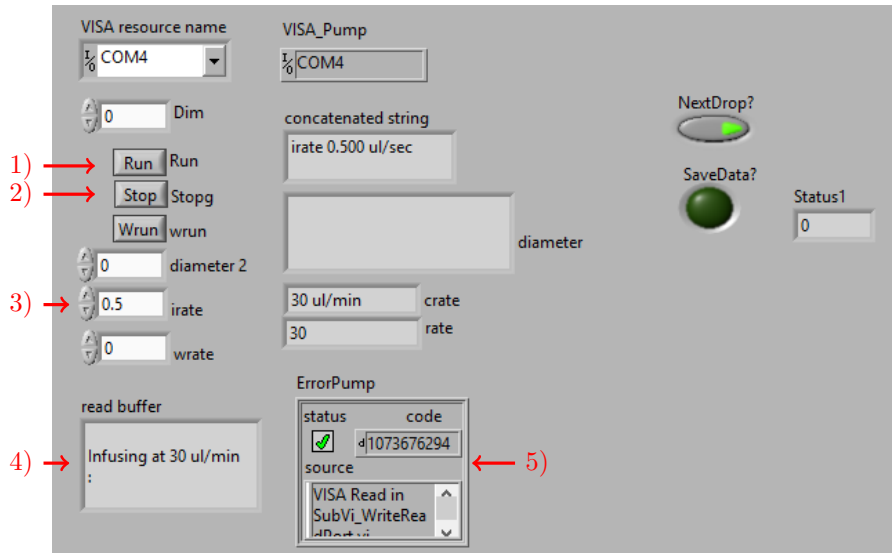

Figure 4.16: User interface for control of the syringe pump.

The flow rate of the oil into the continuous water phase can be adjusted by changing the irate (3). The corresponding volume flow rate the oil is infused at, will be displayed in (4). The status of the pump is shown in (5).

Monitoring the Continuous Phase
In the tab 'ACQ', the flow rate and the mechanical water pump can be monitored. However, the flow rate of the water can only be adjusted by adjusting the pump effect manually on the control panel connected to the pump (explained in section 4.1.2).

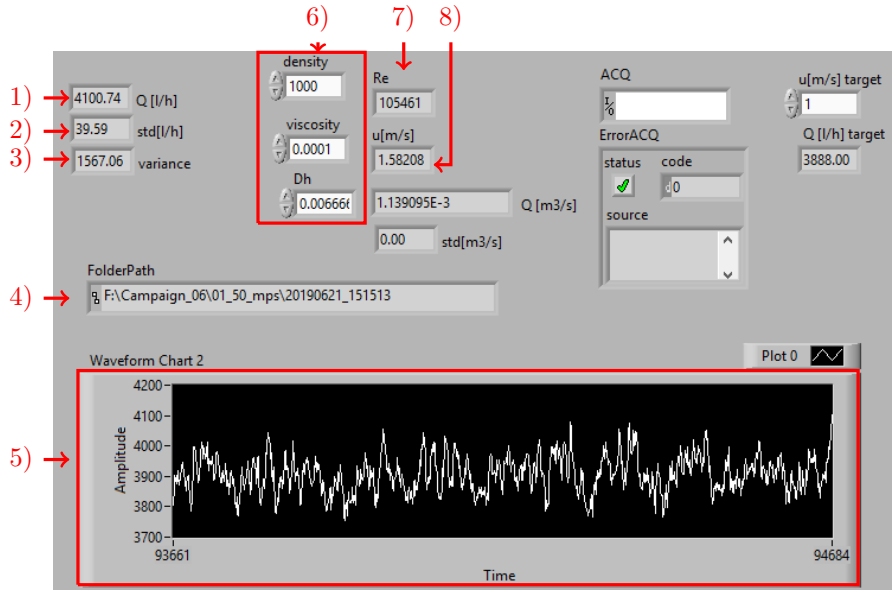

Figure 4.17: User interface for monitoring the mechanical pump.

The volumetric flow rate is displayed in (1) along with the standard deviation (2) and variance (3). The folder path in which the current droplet video is saved is shown in (4). In (5), can the evolution of effect of the pump be monitored. The physical properties of the continuous phase can be adjusted in (6). The Reynolds number for the continuous phase is displayed in (7) and the velocity of the flow is displayed in (8).

4.2 Running Experiments

4.2.1 Start-Up

The experimental setup is started by switching on the lights, the electricity to the pump, the syringe pumps, the acquisition card and the two cameras. A safety valve, keeping the water in the tank from running into to the pipes during downtime, is then opened. The pump is then switched on and kept running on a low frequency until water is flowing through the entire circuit. Then, the power on the pump is adjusted to the maximum, letting the circuit run on max velocity.

The pump should be kept on maximum speed for approximately ten minutes to ensure that any air bubbles trapped in the pipes will follow the high velocity water flow through the pipes and into the water tank. The air bubbles are unwanted in the pipes because they are falsely detected by the software as droplets and disturb the collection of droplet videos. Whilst waiting, the camera settings, the ROI and the syringe pump flow rate are adjusted. This is described in section 4.1.10. After running the circuit on high velocity for approximately ten minutes, the speed of the pump was changed to obtain the desired water flow rate. The pump will need a couple of minutes to stabilize at the desired speed.

4.2.2 Droplet Detection

Live imaging from the cameras have to be switched off whilst droplet detection is carried out. By clicking 'ready acquisition', the software will create a background image as an average of many images from the camera. Oil droplets will be pumped out in the channel at a constant flow rate. The background image will continuously be compared to the images obtained from the camera. When a droplet is detected, the syringe pump stops pumping oil into the channel, while the droplet video is saved. By clicking 'run continuously', the droplet detection process will repeat after completion of saving the necessary material from the droplet detection.

Figure 4.18: User interface for droplet detection.

4.2.3 Storage of Droplet Breakage Data

Whenever a droplet is detected, a new folder for saving the droplet video is created. The folders are sorted by date and time and contain information about a detected droplet. This includes:

- Camera images from the droplet detection, the *droplet video* saved at a frame rate of 4000 fps.
- Text file: 'data.txt', containing information about the water velocity, the

ROI, the temperature of the water etc. An example data text file is given in Appendix B.

- Text file: 'background.txt', containing the pixel values in the background image

4.2.4 Shading

Shading of the cameras should be done approximately every hour whilst running experiments. This is especially important for the first couple of hours of running experiments, because the cameras need some time to 'warm up' during performance. If shading is not executed, the videos will be of worse quality due to dark, vertical stripes appearing on the images. Click on 'Ready Acquisition' to switch off the droplet detection whilst shading. To shade, simply click on 'shading' (see 'Camera Settings' in section 4.1.10), before restarting the droplet detection.

4.2.5 Aspects to Consider

The water flow should be clean without air bubbles, dirt, hair or microorganisms, because this will disturb the detection of droplets. If there are any air bubbles, this can be a result of not having run the water flow at high velocity for a sufficient amount of time during start-up. A possible solution for the problem is to stop the pump and wait for approximately five minutes to let any air bubbles in the pipes rise and collect in the water tank. Run the water flow at high velocity again before turning the frequency of the pump down to the desired level. If there are any hairs, microorganisms or dirt in the systems, the water in the tank should be replaced with fresh, clean de-ionized water. The process is described in Appendix A, 'Maintenance'.

4.2.6 Shut-Down of the Apparatus

Shut-down of the experimental setup can be commenced while the software is saving the last droplet video. Make sure the 'run continuously' function is switched off to ensure no more oil is pumped into the water flow by the syringe pump. Shut-down of the experimental setup is done by running the pump on reverse to remove the water from the pipes and lead the water back to the water tank. The pump is run on reverse until the flow meter shows a strongly decreasing negative flow rate. At this point, the pump is mostly pumping air through the pipes, meaning the water has been pumped back into the water tank. The pump is shut off and the valve between the water tank and the pipes is shut. When the droplet videos are done saving, the 'STOP' button is clicked to exit the software used during experiments. The cameras can be shut off and the lens is covered. The syringe pump and acquisition card are shut off. Finally the lights are turned off.

4.3 Camera calibration

Camera calibration is necessary to ensure that the images from the two cameras overlap correctly. The aim is to allow tracking of droplets' path through the entire channel that is on camera, even in the intersection of the two cameras. The calibration is done in an application-style script in MATLAB, 'Calibration.mlapp'. The output of the calibration is a MAT-file, hereby entitled a *calibration file*. The calibration files are used in the image processing. In order to catch any movement in the position of the cameras or any changes in the camera settings, new calibration files are made for every day of experiments. The user interface for the app is shown in Figure 4.19.

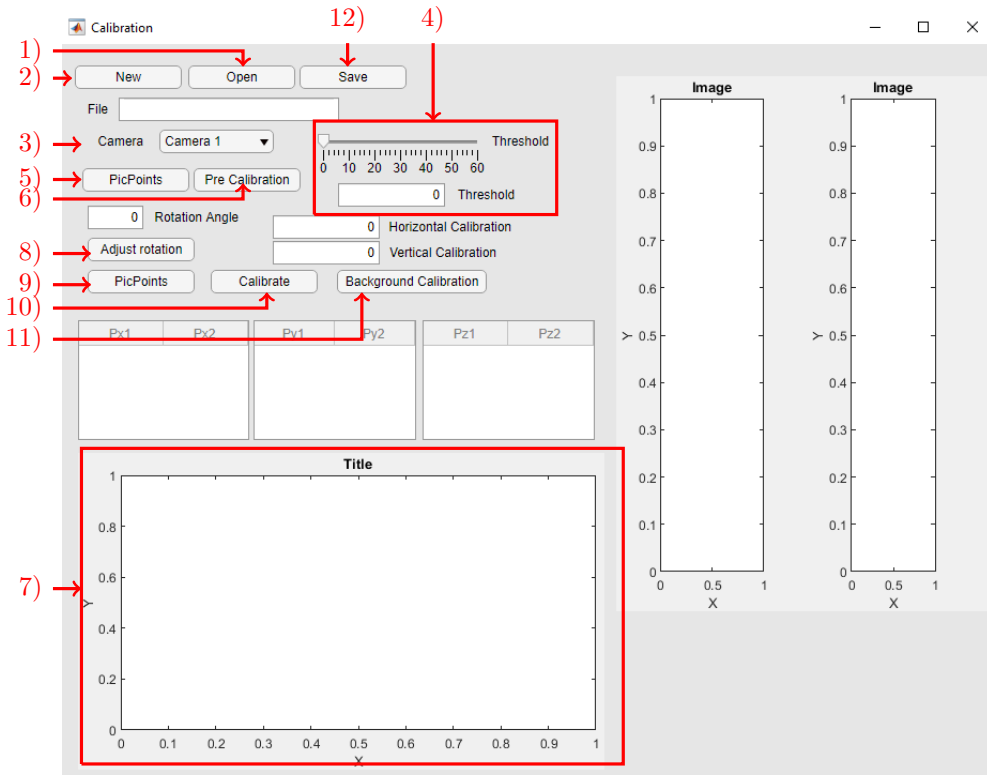

Figure 4.19: User interface for the calibration app.

In the calibration app, it is possible to open already existing files (1) or create new calibration files (2). A new calibration file is created by selecting a droplet file for the specific day that is to be calibrated (3). The steps of calibration are

presented in the flow chart displayed in Figure 4.20. The steps of the calibration is executed for one camera, the repeated for the second camera (4).

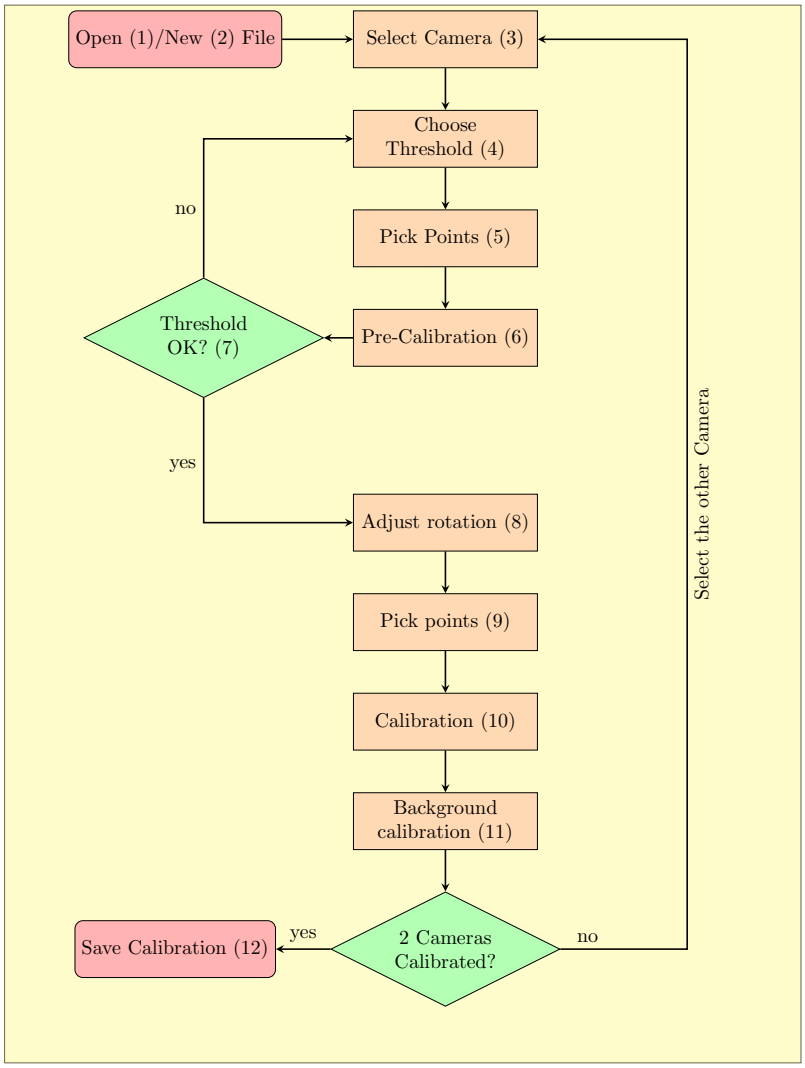

Figure 4.20: Flowsheet for the Camera Calibration.

4.3.1 Threshold

The calibration is done using a binary version of the background image. A binary image is a digital image that consists of pixels with two possible values, usually a black and white image, where 0 represents black and 1 represents white. The background image obtained from the breakage files is a greyscale image with pixel values between 0 and 255, where 0 is black and 255 is white. In the process of converting the greyscale image into a binary image, a threshold value is chosen. The threshold value is the deciding factor if a pixel is converted into black or white.

The threshold value is set by moving the bar next to 'Threshold' (5) (see Figure 4.19). When setting the threshold value, the corresponding binary image appears to the right of the original greyscale image. Figure 4.21 illustrates the effect of the threshold value on the corresponding binary image. Figure 4.21a shows an original greyscale background image. This image is converted into a binary image using two different threshold values, shown in Figures 4.21b and 4.21c.

Figure 4.21c illustrates how the binary image looks like when the chosen threshold is too high. A higher threshold will result in more pixels converted to black. Consequently, the area between the turbulence enhancing metal rods on the channel walls is not clearly defined. Figure 4.21b shows a binary image with a well selected threshold. The turbulence enhancing rods are visible and there are no black areas between the rods.

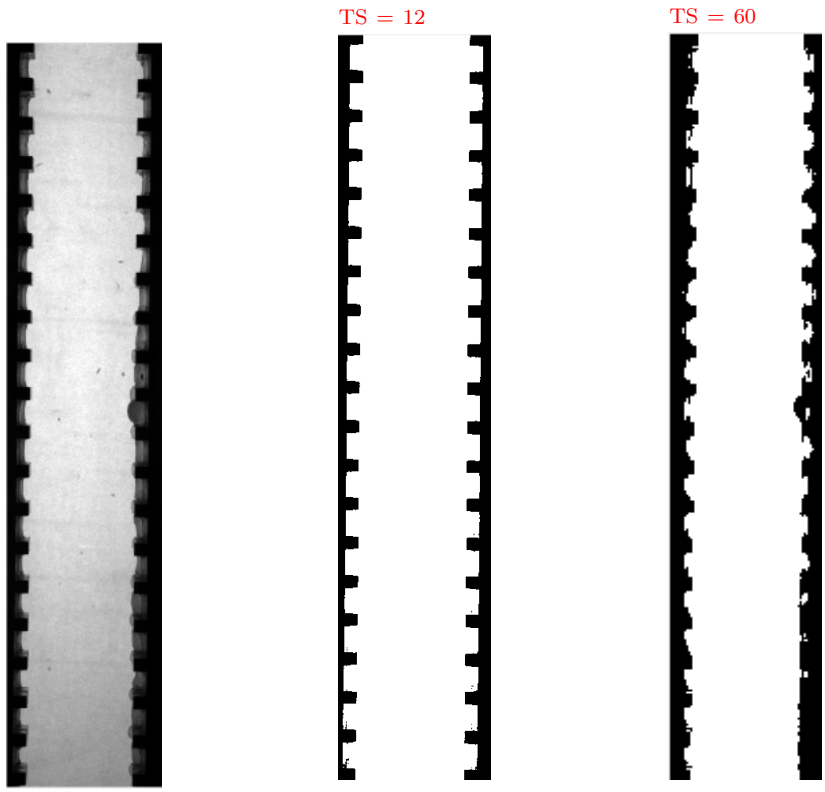

Figure 4.21: Determination of an appropriate threshold value for an example calibration. (a) is the original greyscale background image. (b) is a binary image with a threshold value of 12. (c) is a binary image with a threshold value of 60.

4.3.2 Pick points

By clicking the button 'Pic Points' (6), a new figure is opened. First click on a point between the two bottom turbulence enhancing metal rods, as illustrated by the intersection of the two red lines in Figure 4.22a. Secondly, click on a point between the two top metal rods as shown in Figure 4.22b.

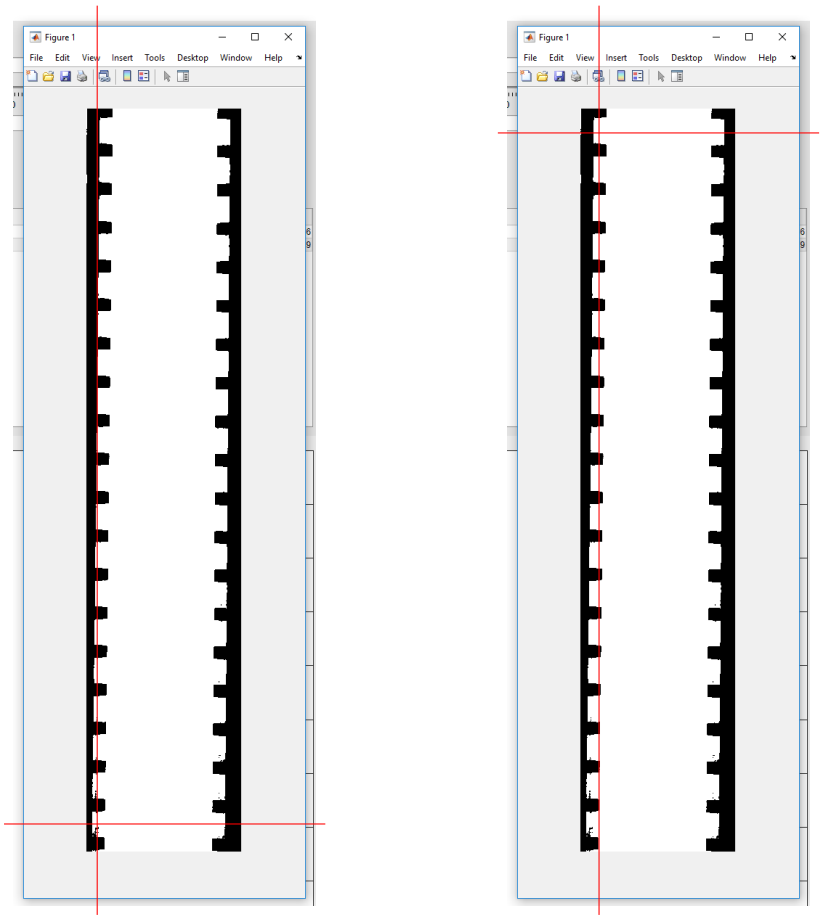

(a) (b)

Figure 4.22: Pick points procedure. (a) illustrates where the first point should be, represented by the intersection of the two red lines. (b) illustrates where the second point should be.

4.3.3 Validation of threshold

The choice threshold value can be confirmed by using a graph similar to the graphs displayed in Figure 4.23. This graph shows up in the calibration app after the pre-calibration in the user interface presenten in Figure 4.19. The pixel value is plotted on the y-axis for pixels in the binary background image. The pixels lie on a vertical line across the turbulence enhancing metal rods, between the two points chosen in section 4.3.2. Since the pixels plotted are from a binary image, the value of the pixel will either be 0 or 1.

For a chosen threshold value, the graph should have alternating blocks of pixels with a value of 0 and 1, representing the metal rods and the area between. This is illustrated in Figure 4.23b. Figure 4.23a shows how the graph would look like if the threshold is chosen too high, indicating that the threshold value should be changed.

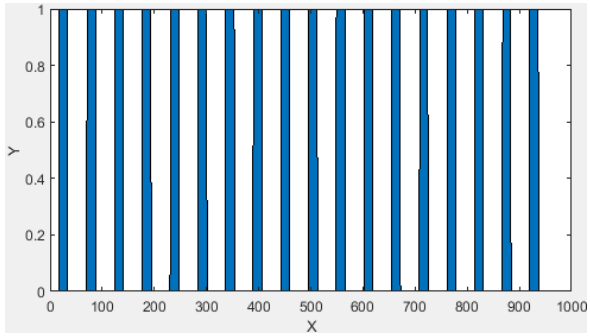

The alternating blocks of pixels with a value of 0 and 1 are clearly defined

(a)

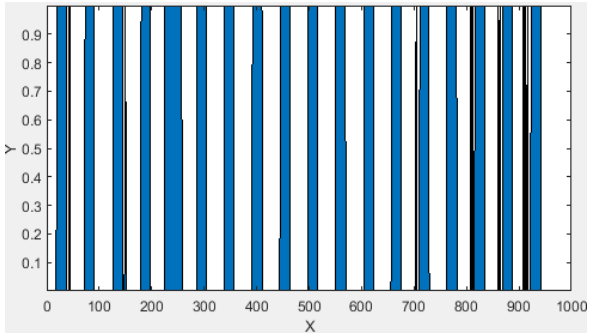

The alternating blocks of pixels with a value of 0 and 1 are uneven

(b)

Figure 4.23: Graph used to validate the chosen threshold value.

4.3.4 Calibration of Perspective

The last step of the calibration is a calibration of the perspective in the photo. This step takes into consideration that the images are a projection of a three dimensional channel onto a two dimensional plane. The calibration of the perspective is done by looking at the turbulence enhancing rods. In the center of the channel, only the side of these metal rods are visible. Due to the perspective, also the top are visible on the metal rods in the bottom of the image. For the metal rods in the top of the image, the bottom of the rod is visible. The length of the metal rods are known (30mm). The background calibration is done by comparing the known length with the length measured for the top and bottom metal rods on the background image.

By clicking on 'Background Calibration', a separate window with the background image will appear. The process of calibrating the background is made easier by zooming in. This is done by marking the area to be zoomed in at and double clicking. The process is illustrated in Figure 4.24.

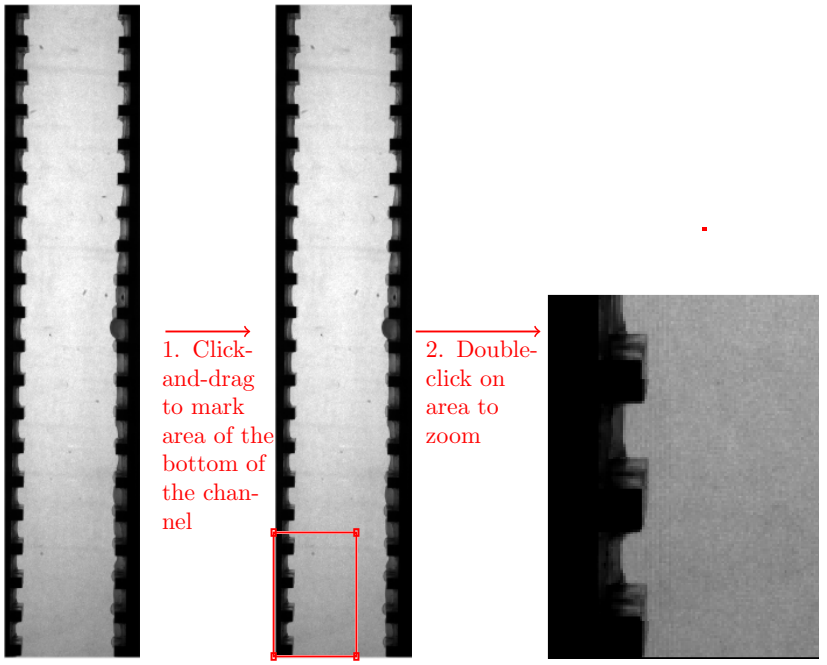

Figure 4.24: Step-by-step illustration of how to zoom in on the corners of the channel.

Click on the front edge of the bottom metal rod, then click on the back edge of the same bottom metal rod. The process is illustrated in Figure 4.25. Repeat the zooming and clicking for the top part of the channel.

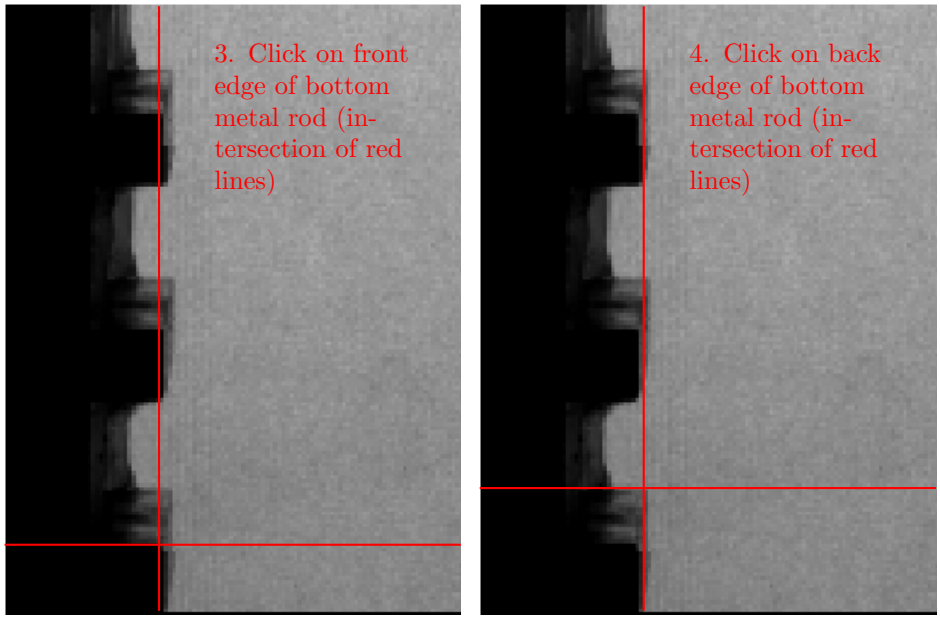

Figure 4.25: Background calibration.

4.3.5 Saving

Save the calibration by clicking on 'Save'. By saving, a new calibration file will be created. The calibration file can be re-opened and edited. This camera calibration file will be used in the image processing, which is to be described in section 5, Image Analysis.

5 Image Processing

5.1 Analysis Overview

Figure 5.1 displays a flow chart for the steps of the image analysis. The analysis is based on the droplet files created in experiments as described in section 4.2, Storage of Droplet Breakage Data. Image processing is carried out in two different application-style scripts, made and used in MATLAB. The final result of the image analysis is a MAT-file in MATLAB, hereby referred to as a 'breakage file'. This file will contain information about the mother droplet and, if there are any, daughter droplets. Such information includes drop size, position, dissipation rate and kinetic energy of the droplets at any position in the channel. For breakage events, the information also includes breakage time and number of daughters.

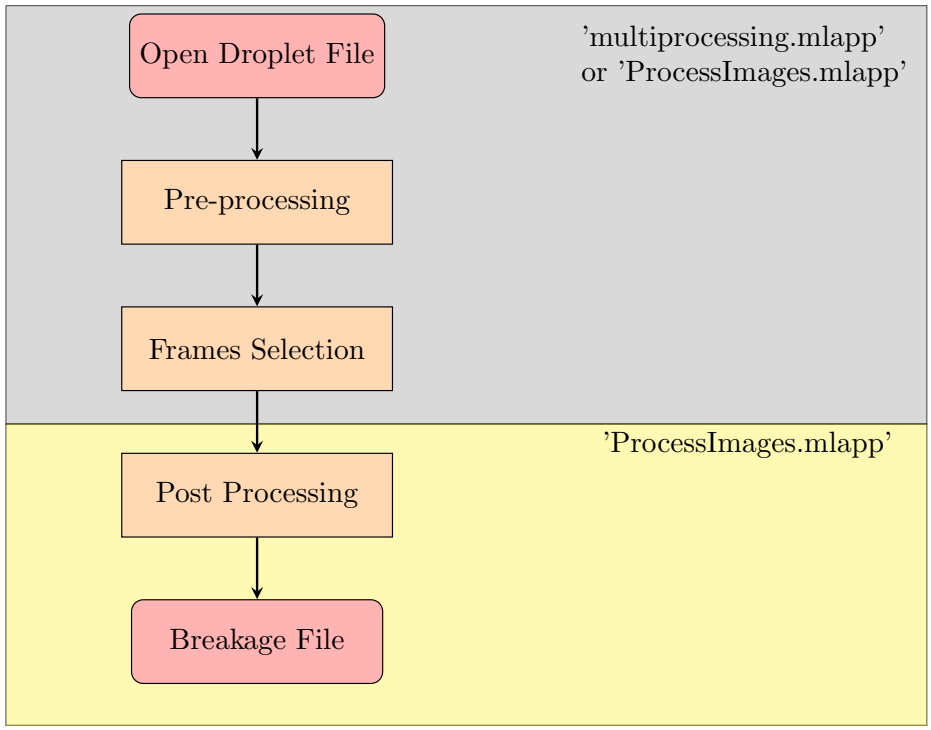

Figure 5.1: Flow chart for the steps of the Image Processing. The steps in the grey box can be executed in both the 'multiprocessing.mlapp' and 'ProcessImages.mlapp'.

5.2 Image Processing Applications

Processing multiple droplet files simultaneously, *batch* processing, is possible in the 'multiprocessing.mlapp'. The user interface is displayed in Figure 5.2. The important features are marked with a number and will be subject to further explanation in this section.

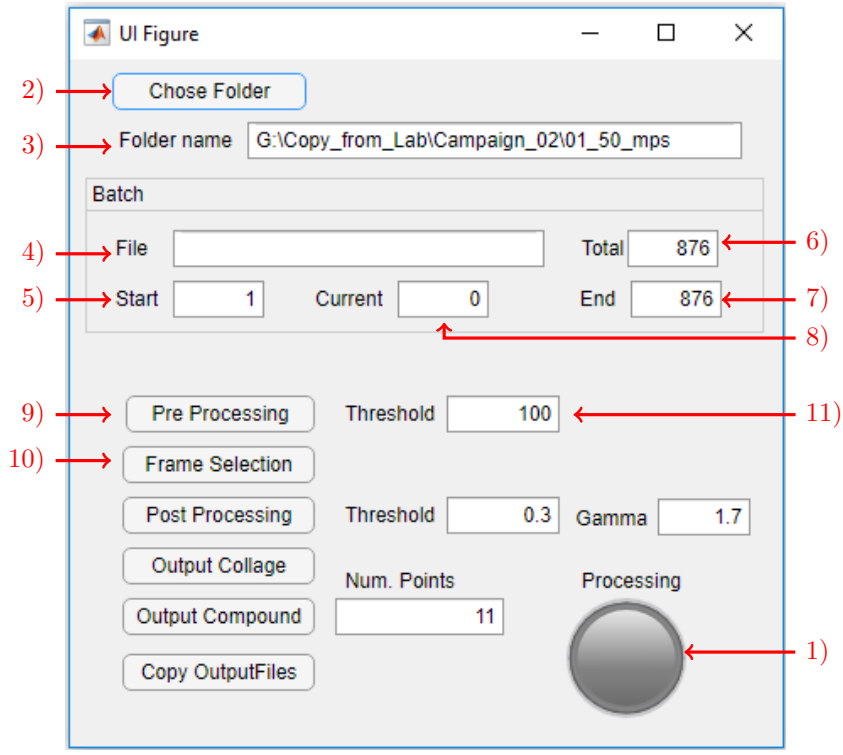

Figure 5.2: 'ProcessImages.mlapp' - User interface for the batch image processing.

A green light (1) indicates that the program is executing a command. The button turns grey when the task is completed. A batch image processing is initiated by choosing a directory (2). The directories are organized into folders, one folder for each velocity of the water flow. After selecting a directory, the folder name will appear in (3). During batch processing, the name of the droplet file under processing will appear in (4). Each droplet file can also be denoted by numbers, and it is possible to see the number of the starting folder (5), the

total number of folders (6), the end folder (7) and the current folder being processed (8). Pre-processing (9) (see section 5.3) and selection of frames (10) (see section 5.4), is predominantly carried out in the batch processing app ('multiprocessing.mlapp'), but can also be done in the single file ('ProcessImages.mlapp') processing app.

The interface of the single droplet file processing application, 'ProcessImages.mlapp', is shown in Figure 5.3. The main purpose of the single droplet file processing app is the post-processing.

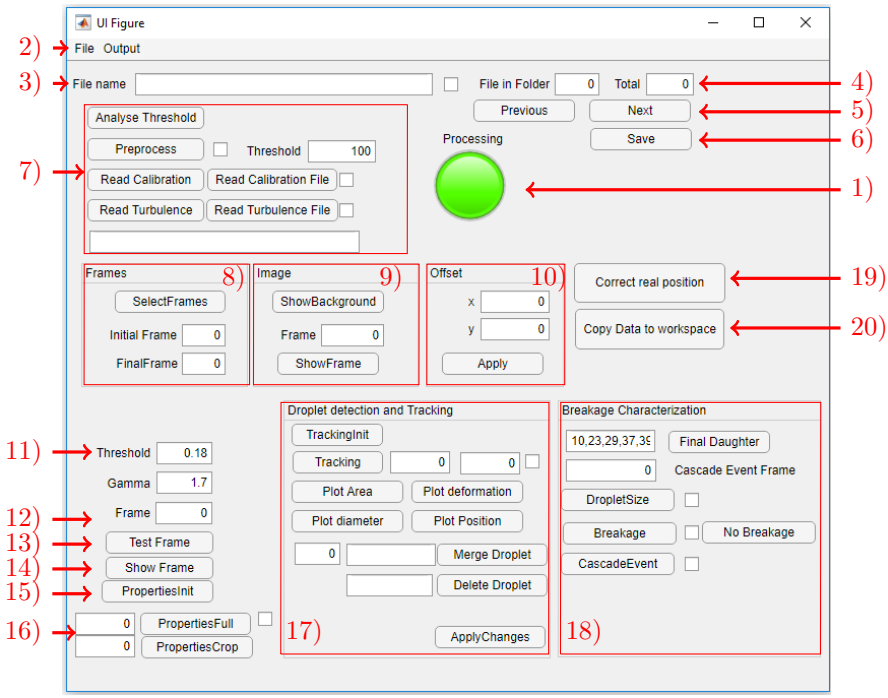

Figure 5.3: User interface for the single file processing 'ProcessImages.mlapp'.

A green light (1) is switched on whenever command is executed and turns grey after completion. Under file (2), a new file can be created by clicking 'new' and an existing file can be reopened by clicking 'open'. The name of the file being processed will show up in (3), in conjunction with the file number in the folder and the total number of files in the directory in (4). Moving back and forward between droplet files can be done by clicking 'previous' and 'next' (5). Click at (6) to save any changes.

By choosing 'new', the unprocessed droplet file will be opened, meaning all the steps of the image processing has to be completed, including the pre-processing (7) (section 5.3) and frames selection (8) (section 5.4).

In (9), there is the possibility to show the background image used in the analysis. An example background image is presented in Figure 5.4a. By clicking 'Show Frame', the frame with the given frame number will be displayed, both as the original frame (Figure 5.4b) and the frame subtracted the background (Figure 5.4c).

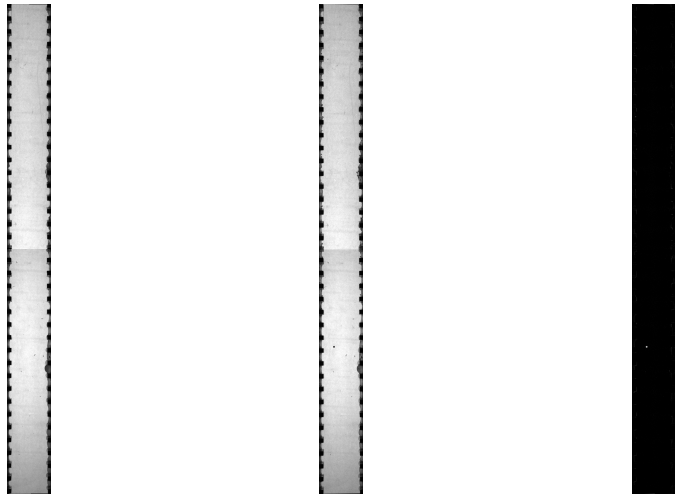

(a) Bakground image (b) Show frame (c) Frame with background subtracted

Figure 5.4

The offset can be adjusted in (10). This function, along with the adjustment 'Threshold' and 'Gamma' in (11) is elaborated later in section 5.5.1, Image Properties. 'Test Frame' (13) and 'Show Frame' (14) are used to show the detection of droplets in a chosen frame. Use 'Test Frame' whenever a property is altered, such as the offset or the threshold, to verify the changes. 'Show Frame' is used after the properties are permanently adjusted.

The properties are determined by first initializing the properties by clicking 'PropertiesInit' (15) and then iterating through the frames (16), detecting the new properties. The tracking and manipulation of the tracking are done in (17) (explained in section 5.5.2) and the finalization of the breakage files is done in (18) (explained in section 5.5.4).

5.3 Pre-Processing

Pre-processing starts by choosing a turbulence file. The turbulence files contain information about the turbulent flow in the breakage channel. The files are made from performing a breakage characterization (La Forgia et al. [34]) with Laser Doppler Velocimetry in the channel at different velocities of the continuous flow. The velocity in the turbulence file should match the velocity of the flow in the droplet files. Information from the turbulence file will be matched with the position of the droplet later in the tracking, ensuring that it is possible to obtain the dissipation rate and the kinetic energy of the droplet at the different positions in the channel.

Choose the appropriate calibration file. The calibration files are used to combine the frames from the two cameras to one, long image of the breakage channel in such a way that the two images overlap correctly.

The pre-processing will commence automatically after selecting the turbulence and calibration files. If the pre-processing is done in batch, it will iterate through all the folders in the directory until all the droplet files are processed.

5.4 Selection of Frames

The purpose of the frames selection process is to select a frame interval in the droplet video files, where there are droplets detected. The process involves selecting a start frame and a final frame. In the post-processing (section 5.5) the entire frame interval will be used unless otherwise specified.

To identify frames with detected drops, the frames selection process uses a background image to compare to the frames in the droplet files. For each frame in a file, the background image is subtracted. The resulting image shows the difference in a frame from the background image. If a frame is identical to the background image, the resulting image would be completely black. However, if there is a droplet in the image it would show up as a lighter area in the resulting image. The subtracted image is then converted into a binary image. This way, if there are any droplets in the frame, they will appear white on a black background in a binary image. Vibrations in the channel and dust particles flowing through the channel will also show up as white areas in the binary image, thereby causing some noise. Nonetheless, the number of white pixels in the resulting image could be used as an indication of detection of droplets.

Figure 5.5 presents an example graph where the number of white pixels in the resulting image is plotted chronologically against the frame number. The blue data indicates a detection in camera 1, whereas the red data indicates a detection in camera 2. The figure shows how the first part of the image contains some noise or vibrations. Then, there is a drastic increase in the number of pixels different from the background in camera 1. When the number of detected pixels decreases

for camera 1, the number of pixels detected in camera 2 increases. The increase is an indication of a droplet entering the channel. The transition from the peek in camera 1 to the peak in camera 2 shows where the droplet exits the view of camera 1 and enters camera 2.

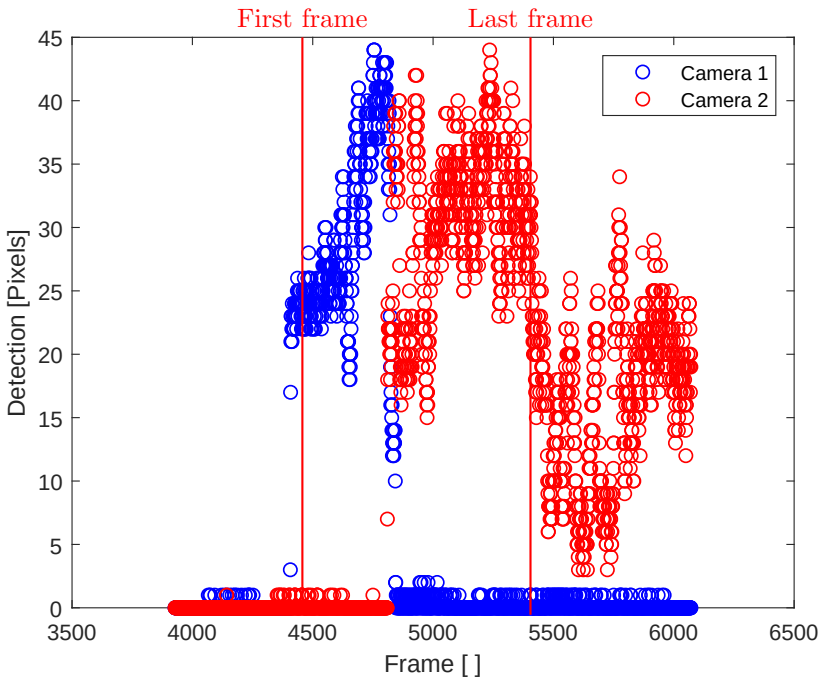

Figure 5.5: Frames Selection for example droplet file.

In Figure 5.5, click where the first frame should be. The frames selection is only considering the frame number, so the position on the y-axis is indifferent when clicking. The first frame should be around 10 frames after a droplet is detected in the first camera. Make sure that the first frame is not chosen before the droplet has entered the channel, as this will cause problems in the tracking. A red line indicates where to click on the graph. Then, click where the last frame should be. The last frame should be chosen such that the entire breakage is caught on tape.

5.5 Post-Processing

A flow chart of the post-processing is shown in Figure 5.6. Post-processing can only be initialized after pre-processing and selection of frames is completed.

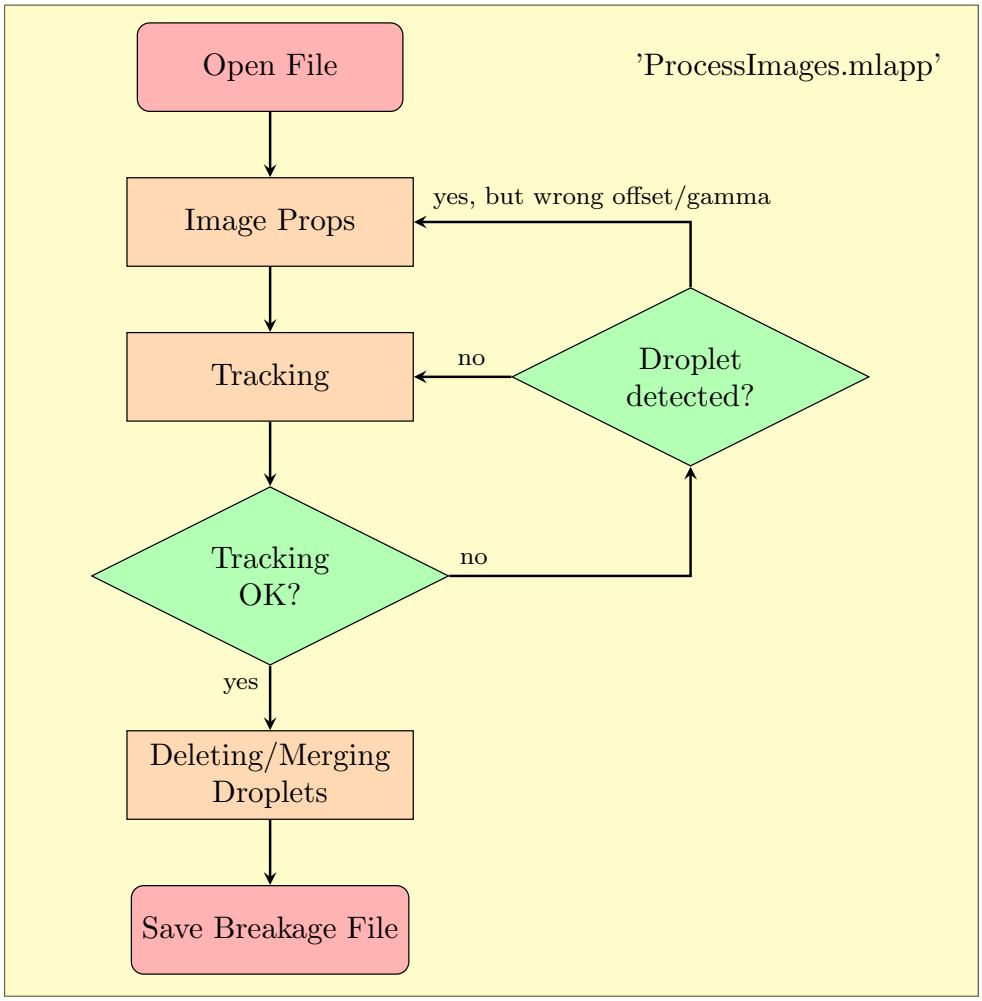

Figure 5.6: Flowsheet showing the steps of image post-processing.

5.5.1 Image Properties

The first step of post-processing is to detect droplets and find the properties of these droplets. This involves iterating through all the frames to find any droplets and decide their position in the channel, their area, and centroid.

Detecting droplets is done by comparing the frames to a background image without a droplet. The background image is subtracted from the frame. Any droplets in frame will appear white or light gray on a black background. A threshold value decides at what intensity a pixel is interpreted as a part of a droplet. When a droplet is identified, information about the position and size is saved. This information is combined with information from the turbulence file. A pixel limit of 4 pixels is applied to remove any noise from the subtracted image. If there are any droplets smaller than 4 pixels, they have to be added manually in the manual breakage file (see section 5.6).

Figure 5.7 displays a cropped version of the interface for the single file processing app, used for the detection of droplets.

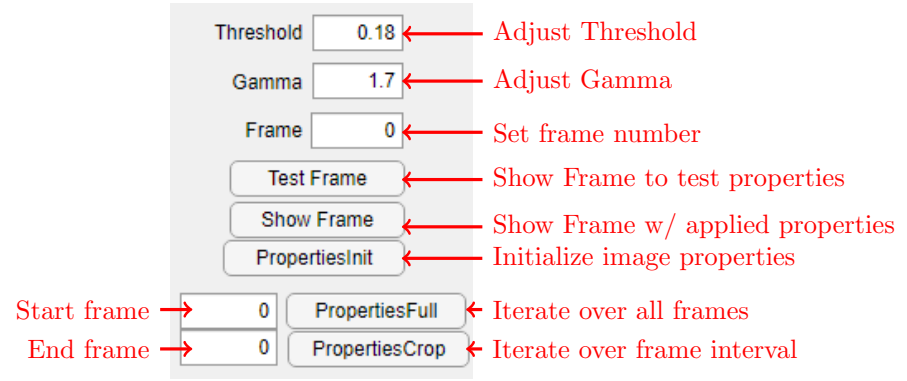

Figure 5.7: Crop of user interface of the 'ProcessImages.mlapp' used for the image properties

By clicking at 'Properties Init', the image properties are reset and the droplet properties detection can start. By clicking 'Properties Full', the program iterates from the first frame to the last frame. Alternatively, it is possible to iterate through a selected interval of frames by writing the wanted start frame and end frame and clicking 'Properties Crop'.

The image properties are affected by the offset values and the threshold and gamma values. To find out if these properties need adjustment, it is necessary to look at the result of the tracking.

Effect of the offset: An assumption used in the camera calibration (section 4.3) is that the droplets move in the center of the channel. This assumption is naturally often an erroneous assumption, as a droplet could be positioned anywhere in the channel. If a droplet passes the joint between the cameras anywhere else than the centre of the channel, the overlap of the images might result in the droplet disappearing, being misshaped or too large in the frames from the intersection. This can be detected by plotting the droplet area as a function of the frame number after the tracking (will be explained in section 5.5.2). Figure 5.8 displays an example of said graph. Around frame 4950, there is a drastic decrease in the area of the droplet. This can imply that the offset value should be changed.

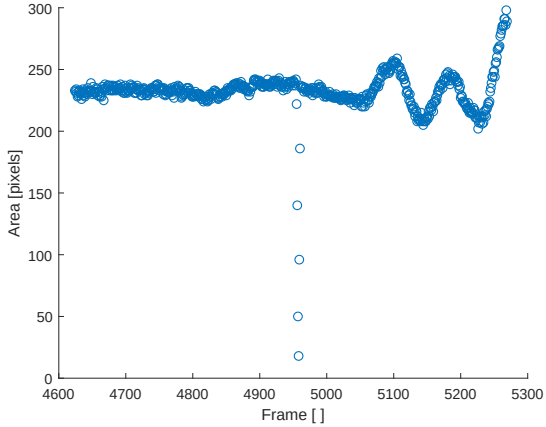

Figure 5.8: Droplet area for a single droplet plotted as a function of the frame number.

In Figure 5.9a, a frame of the mentioned droplet, from the plot of the droplet area in Figure 5.8, is displayed at the intersection between the cameras. The default offset values of 0 in the x-direction and 0.25 in the y-direction are used to create this image. In this specific instance, a large fraction of the droplet is lost at the intersection due to the offset value. By changing the offset value to 0.1 in the x-direction and -0.8 in the y-direction, the entire droplet is visible in the intersection, as shown in Figure 5.9b.

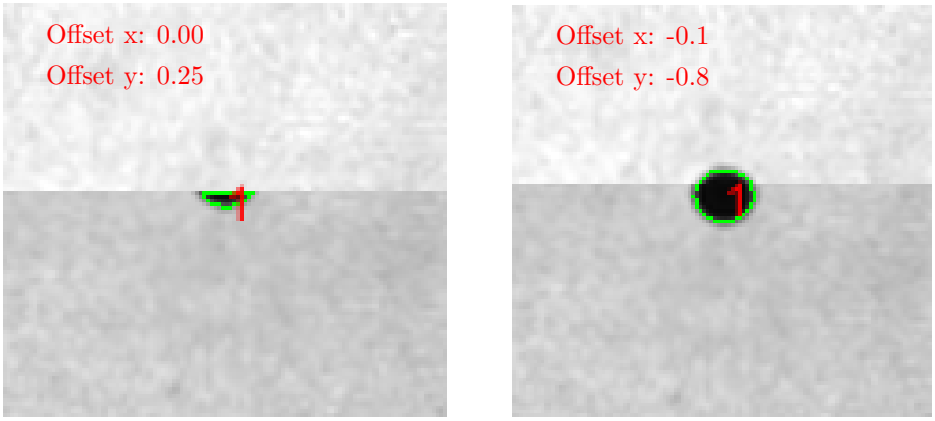

(a) (b)

Figure 5.9: Droplet at the intersection between cameras using different offset value.s

Effect of gamma: The gamma value is a determining factor for what should be interpreted as a droplet. When the background image is subtracted from the frames, the resulting image will have a black background with the droplets as lighter areas. The intensity of the lighter areas is higher for larger droplets, because the larger droplets appear darker in the water than the smaller drops. The gamma value determines what intensity of the lighter areas should be interpreted as a droplet.

By using a high gamma value, less will be interpreted as a droplet. There is a possibility of loosing information, such as small droplets. By choosing a lower gamma value, more of the darker gray areas will be interpreted as a droplet. This might result in small vibrations or movement close to the wall being detected as a droplet, which can cause a large amount of manual labor later (see section 5.5.3, Merging and Deleting Droplets).

5.5.2 Tracking

The tracking connects all of the information about the detected droplets in every single frame to each other. After completing the tracking, the result is a suggestive path of the mother droplet, the point of breakage, the path of the daughters and any cascade breakage events. A cropped version of the user interface for the 'ProcessImages.mlapp' with the functions necessary for completing the tracking is displayed in Figure 5.10.

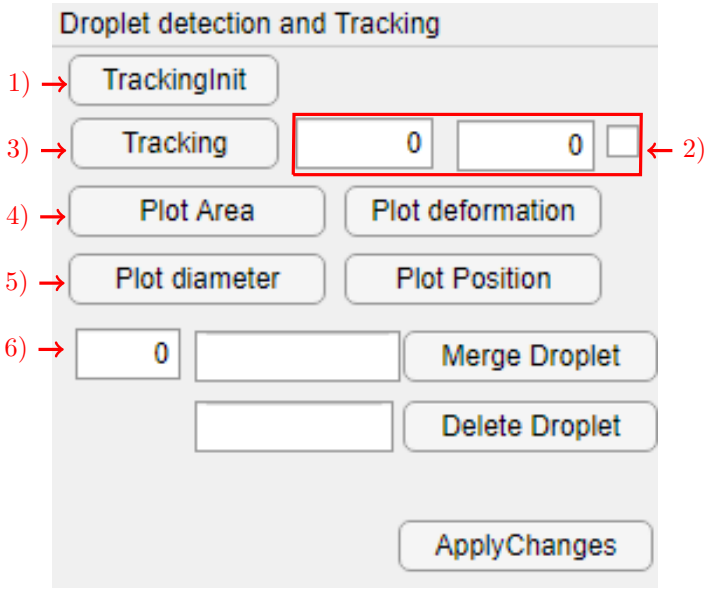

Figure 5.10: Cropped version of the interface of 'ProcessImages.mlapp' used for the tracking

The tracking itself consist of only two steps:

1. Initialize the droplet tracking, by clicking 'TrackingInit' (1).

2. Choose the frame interval (2) for the tracking and start the tracking by clicking 'Tracking' (3). Usually, a good starting point is to select the start frame and end frame from the frames selection, described in section 4.3.2. If the tracking does not detect any droplets, it could be due to the fact that the starting frame is chosen too early.

   The tracking searches for a droplet at the entrance of the channel. If the entire droplet has not completely entered the channel, the tracking might

falsely interpret vibrations at the entrance as a droplet and thus not detect the actual droplet. The problem could be solved by re-initializing the tracking and start the tracking with a new starting frame.

Droplets hitting the wall prior to, or during the breakage event may result in a multitude of droplets. Wall breakage combined with a large number of daughter droplets can be a challenge for the tracking. Firstly, the contact between the droplet and the wall is difficult to track. Secondly, the many small daughter droplets formed in the breakage event will often disappear and possibly re-appear, being interpreted as a new drop. A solution to reduce the number of droplets detected is to track a shorter time interval by stopping the tracking just after the cascade breakage. This ensures that the manual labor of deleting and merging drops is reduced, yet, no information about the breakage is lost.

Following the completion of the tracking, it is possible to plot various graphs to validate the success of the tracking. Unsuccessful tracking can be caused by wrong offset or gamma (see section 5.5.1, Image Properties) or complicated wall breakages. The plots are useful tools for the process of merging and deleting droplets (see section 5.5.3, Merging and Deleting Droplets) because they can be used to follow the evolution of the breakage event. Example plots are shown in Figure 5.11.

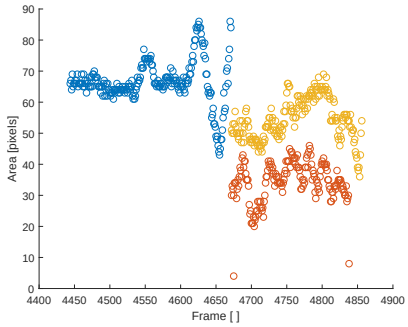

(a) Droplet area plotted chronologically as a function of the frame number

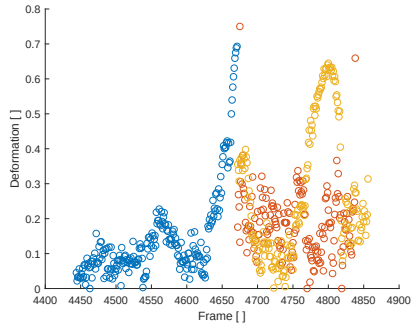

(b) Droplet deformation plotted chronologically as a function of the frame number

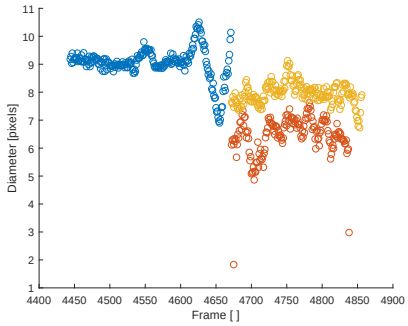

(c) Droplet diameter plotted chronologically as a function of the frame number

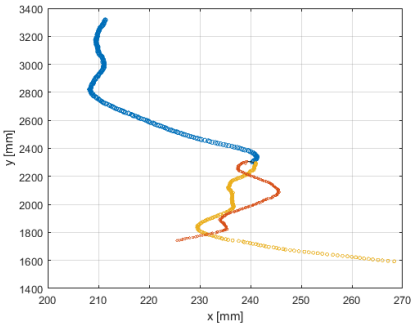

(d) Droplet position in the breakage channel with x illustrating the position in the horizontal direction and y is the position in the vertical direction.

Figure 5.11: Plots obtained from the droplet tracking. Each droplet is represented by a different color.

Figures 5.11a, 5.11b and 5.11c are plotted with the frame number on the x-axis. They show how droplet properties - area, deformation and diameter respectively - manifests itself in the time perspective. Figure 5.11d illustrate how the breakage event evolves in the spatial coordinates. In all four plots, each detected droplet is identifiable by a color and a droplet ID.

5.5.3 Merging and Deleting Droplets

The tracking presents a suggested evolution of a droplet's path through the breakage channel. For certain droplet files, this suggestion is a good match with the actual event. If the tracking and event on the droplet video is a good match, merging and deleting is unnecessary. For other files, the tracking needs some alteration. The process of merging and deleting is best illustrated using an example. Figure 5.12 shows an example of the droplets' pathway through the channel. The mother droplet, droplet 1, breaks in a binary breakage into droplet 2 and 3.

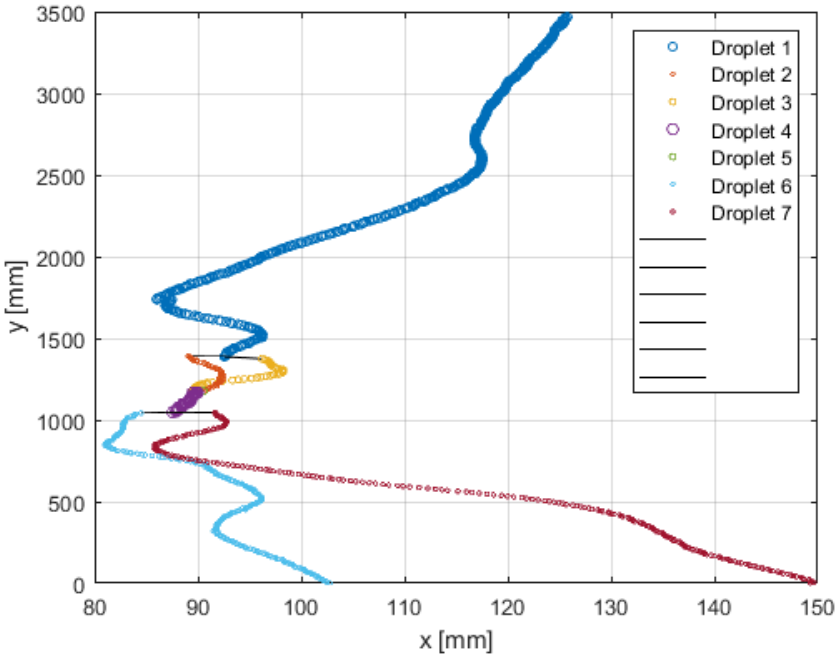

Figure 5.12: Example droplet position plot where one out of two daughter droplets overlap the other daughter droplet. The tracking interprets the overlapping droplets as a new droplet.

After the initial breakage, the tracking loses track of the daughter droplets from the initial breakage, droplet 1 and 2 and detect a new, larger droplet 4 and a smaller droplet, 5. Most likely, these are not new droplets, but a result of the two droplets are moving in the same path, one in front of the other, and therefore being detected as only one droplet. Thus, the two new droplets formed from droplet 4, droplet 6 and 7, possibly are the daughters from the initial breakage. The theory is confirmed by looking into the frames from the droplet file. A few, chosen frames are presented in Figure 5.13. The first frame at t = 0ms, there is only one stable droplet that starts deforming and breaks. After separation, the two droplets start moving closer together. From t = 23ms to 29.5ms, the two daughter droplets are detected as one droplet, before they eventually start moving apart from each other.

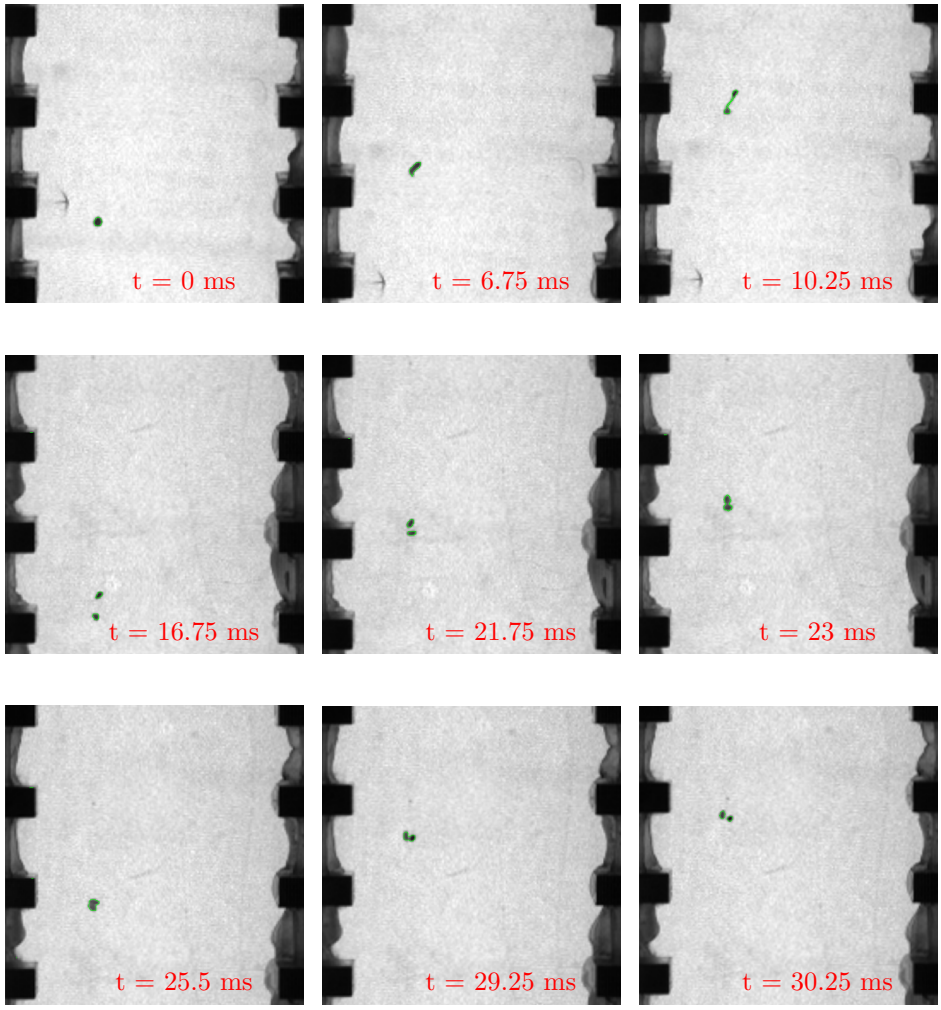

Figure 5.13: Frames from a droplet video showing the evolution of a breakage where the daughter droplets move in the same path, overlapping each other and is therefore detected as one droplet.

The result from the tracking requires some manual alteration. This is done by deleting and merging droplets. In the example presented in Figure 5.12, droplet 4 is deleted, because it consist of both of the daughter droplets. Droplet 2 is merged with droplet 5 and 6. Droplet 3 is merged with 7. The merging and deleting is done in the same user interface as the tracking. The droplet ID of the droplets that are to be merged or deleted are entered into the app (see the user interface in Figure 5.3). By clicking 'Delete Droplet' or 'Merge Droplet', followed by 'Apply Changes', the changes are completed. The end result is portrayed in Figure 5.14.

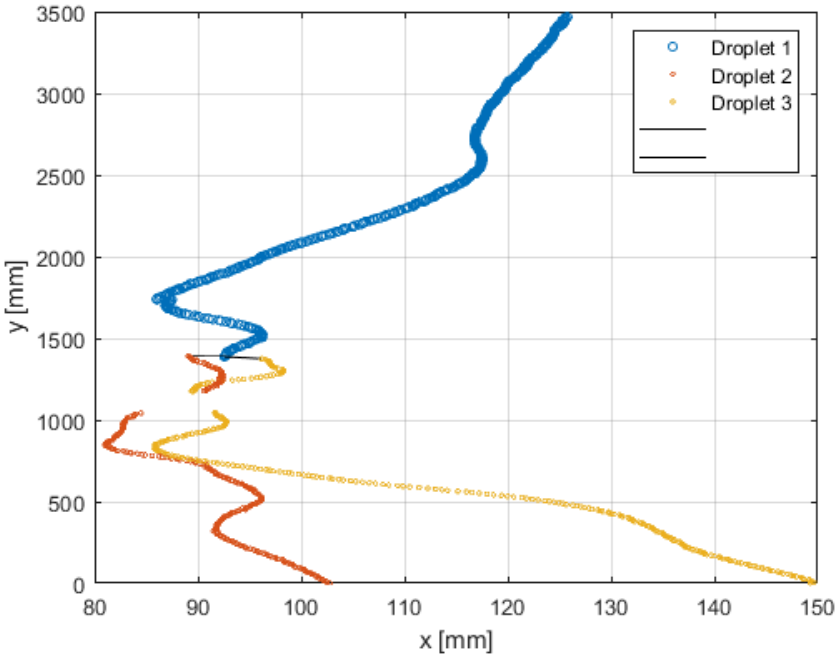

Figure 5.14: Corrected droplet positions.

Figure 5.14 illustrates, correctly, a breakage into two new daughter droplets. There is a gap in the tracking, where the two droplets overlap each other in the frames, however, the breakage file will not be greatly affected by this. More importantly, the breakage file will contain the correct information on the breakage time and the number of daughters. This information would have not been correct if the merging and deleting of droplets was not carried out.

Deleting droplets is also done when multiple breakage events occur in one

file. A breakage is considered to be a part of an event if the droplet has been unstable ever since the formation (due to breakage) or has existed for more than 100 frames. A deformation plot is used to determine whether or not a droplet has been stable. The criteria for a stable droplet is discussed in Appendix C.

If a daughter droplet is found to stabilize after formation, before deforming and breaking, the breakage is considered as a new event. The breakage has to be deleted from the file, to not cause any errors due to a wrong breakage time and number of daughter droplets. The breakage is deleted by deleting the daughter droplets generated from that particular breakage.

For cases where the mother droplet breaks into many small droplets, the daughter droplets might be so small that the tracking has problems detection the droplets. In specific cases, small daughter droplets might be detected for a couple of frames, then disappear, before reappearing again. These droplets might be quite tedious to merge, because they require some detective work to find out where they go. For these particular cases, the most time sparing solution can be to delete all of the tiny daughter droplets, to then add them back to the final distribution using the manual tracking. This method will be explained further in section 5.6.

5.5.4 Breakage Characterization

After tracking, deleting and merging of droplets is completed, the next step is to finalize the post-processing and save the breakage file. The breakage characterization is done in 'ProcessImages.mlapp'. A cropped version of this application is displayed in Figure 5.15. The steps of the breakage characterization are marked with numbers in the figure and will be explained further.

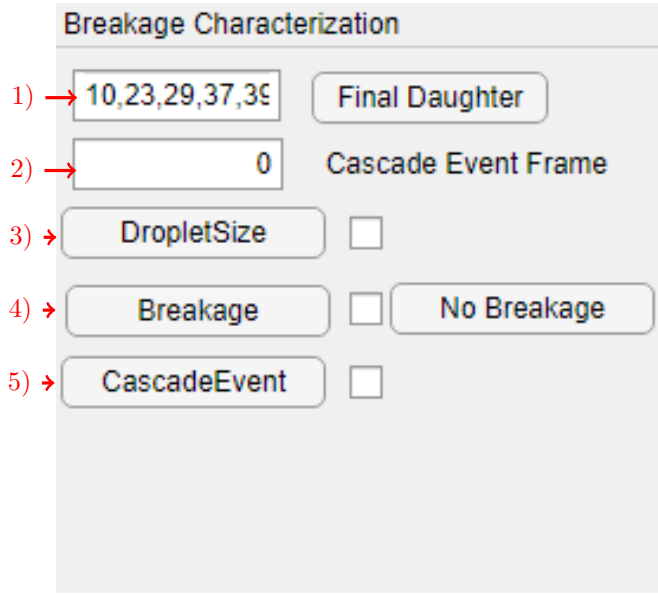

Figure 5.15: Crop of the interface of the 'ProcessImages.mlapp' used for the breakage characterization

1. The first step is to find identify the final daughter distribution. The final daughter distribution consist of the population of droplets after the breakage event is concluded. All the droplets that have existed during the breakage event are identifiable by an ID number. This ID number is used to set the final distribution. The ID number can be found by looking at the droplet position plot, such as the one found in Figure 5.16.

Figure 5.16 shows the position of the mother and daughter droplets. The x-axis represents the position in the horizontal direction in the channel, where the channel walls are at 0 and 300 mm. The y-axis represents the vertical direction, but the position is flipped upside-down. At 3500 mm, the mother droplet (distribution found in data 1) is entering the bottom of the channel. The droplets exit the camera view just after 0 mm. The droplet IDs can be found in the legend of Figure 5.16. The final distribution for this particular breakage is data 2, data 4 and data 5.

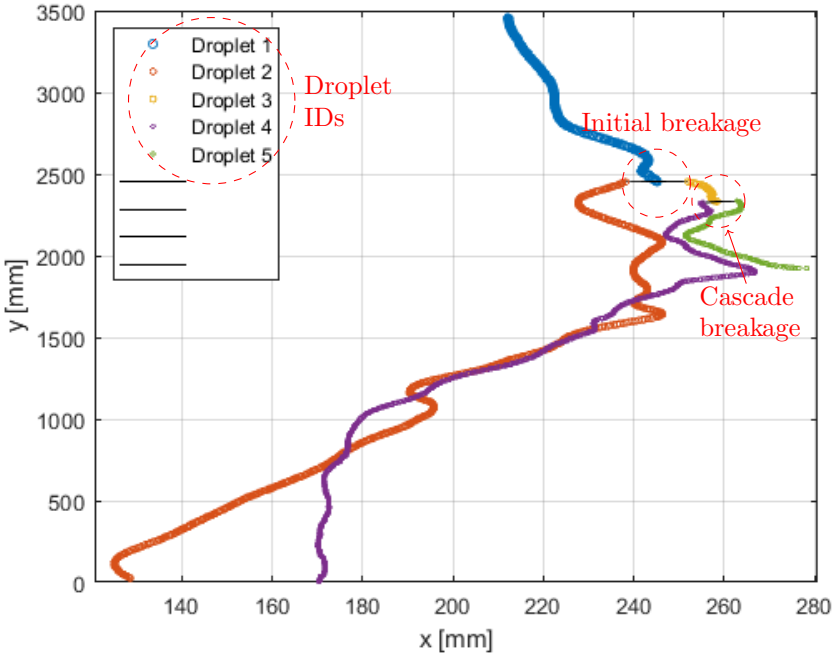

Figure 5.16: Droplet position in the breakage channel

2. The program will automatically find the cascade event frame, when the final daughter distribution is determined. The cascade event frame marks the last frame of the cascade breakage, as shown in Figure 5.16. The cascade event frame can also be set manually.

3. The droplet area will be used to calculate the droplet diameter under the assumption of a spherical droplet. The area for all droplets is saved for every frame the droplet exists. The area is a calculated average of the droplet area in all the frames. However, during deformation of a droplet the droplet area increases. Including the area of a deformed droplet, would give a higher average area. The most correct way to calculate the droplet area is thus to extract the area from the frames where the droplet is stable and has a spherical shape. In Figure 5.17, the normalized area and diameter as well as the deformation of a mother droplet is plotted chronologically as a function of the frame number. In Figure 5.17, the first and last frames are marked by two red lines. Between those two frames, the droplet should be circular and stable. The criteria for a stable droplet can be found in Appendix C. Calculating the average droplet area using areas between these two selected first and last frames, would give a more correct area for a droplet assumed to be circular.

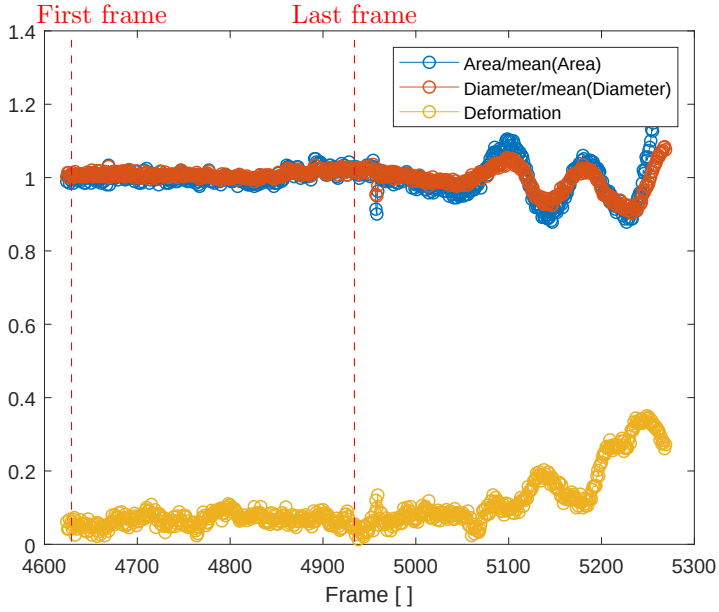

Figure 5.17: Graph for extracting droplet areas. The relative area, diameter and the deformation is plotted chronologically as a function of the frame number.

4. The droplet breakage files contain a boolean value for breakage, that is true if the droplet breaks and false when the droplet does not break. Choose 'Breakage' if there is a droplet breakage and 'No Breakage' otherwise. If there is a breakage, the breakage time has to be determined. A graph with the mother droplet area plotted as a function of the frame number is used for the breakage time determination. Figure 5.18a shows an example of such a graph.

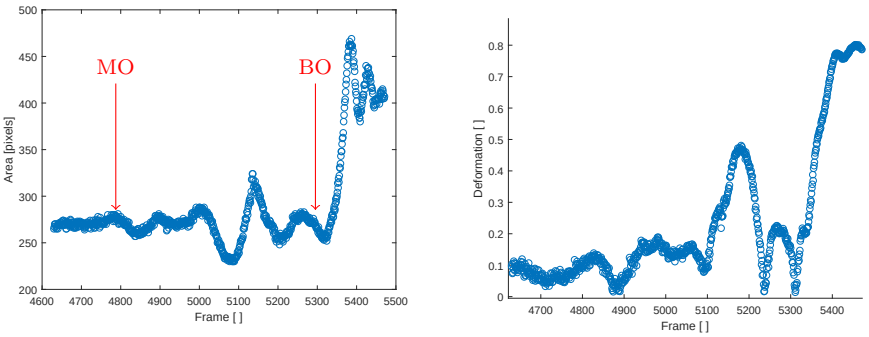

(a) Mother droplet area plotted chronologically as a function of the frame number.

(b) Mother droplet deformation plotted chronologically for all droplets as a function of frame number.

Figure 5.18

Figure 5.18a illustrates one example for droplet breakage time determination. This graph is used to identify the main oscillation, MO, and the breakage oscillation, BO. The main oscillation frame is the first frame of any oscillation of the mother droplet. The breakage oscillation frame is interpreted to be the last frame the the mother droplet is stable and not deformed. Both are marked by arrows in the graph. Notice that the BO point (at around frame 5300) is the last point, where the deformation is zero. Criterias for droplet stability is further elaborated in Appendix C.

In the window with the graph of the mother droplet area, click at the point where the main oscillation starts, then click at the point where the breakage oscillation starts. A deformation plot, as shown in Figure 5.18b, can be useful for the process of finding the start of the breakage oscillation. The breakage oscillation and main oscillation may occur at the same time, if there is only one oscillation before breakage. In Figure 5.19, there is only one, single oscillation before breakage.

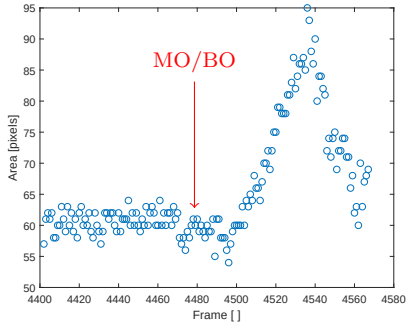

(a) Mother droplet area plotted chronologically as a function of the frame number.

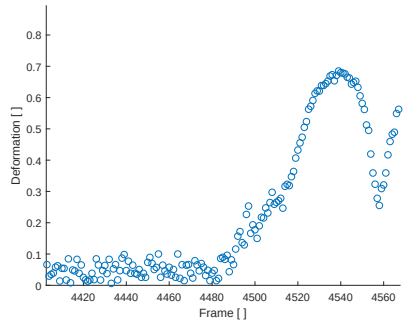

(b) Droplet deformation plotted chronologically for all droplets as a function of frame number.

Figure 5.19

Assuming droplet breakage occur due to only one turbulent interaction, the breakage oscillation is used to calculate the breakage time. The formula for calculating the breakage time is given below:

$$t_b = \frac{\text{Number of frames between BO and breakage}}{\text{Camera record rate}} \tag{18}$$

The camera record rate used in the experiments is 4000 frames per second.

5. Click on 'Cascade Event' if the initial breakage is different from the final breakage. Finally, press the 'save' button to save the changes in the droplet properties and tracking for further use.

5.6 Manual Processing of the Breakage

The image analysis can be a time consuming process. The process of finding the image properties and the tracking can take up to several minutes due to the large amount of data. The deleting and merging of droplets are also time demanding tasks. Consequently, the analysis of a single file can take up to one hour. To reduce the spent on the analysis, adjustments to the breakage file information can be done manually after saving.

One adjustment that is possible to do manually after the breakage is to change the breakage time. The starting point of the breakage is already chosen manually in the finalization of the breakage file in the breakage characterization. The final point of the breakage is by default the point where the mother droplet does not exist anymore. This will vary depending on the chosen threshold value. To adjust the threshold and reset the image properties takes time. Therefore, it is also possible to change the breakage time manually.

Another possibility is to add droplets. Some droplets are not detected by the tracking due to the gamma value and the pixel limit for the size of droplets. Other droplets are deleted to simplify the tracking. These can be added after the breakage characterization in the manual processing.

6 Results and Discussion

A study of single droplet breakage has been performed in an experimental setup using high-speed imaging, as described in section 4.2. The footage from the cameras, the droplet files, have been processed and analyzed using a combination of digital tracking and manual interpretation. The results from the image processing are saved in breakage files, to be used in statistical analysis.

6.1 Dissipation rate

The turbulent flow is critical for the characterization of the breakage because it is assumed that the droplet breakage is caused by a turbulent eddy hitting the droplet. Thus, the turbulent flow criteria have to be fulfilled in order to use the models presented for the droplet breakages. Turbulent flow characterization for the breakage channels was performed by La Forgia et. al [34].

Figure 6.1a displays the breakage oscillation (BO) dissipation rate [m^2s^{-3}] plotted versus the mother droplet diameter. The point of BO is determined to be the last point before the mother droplet starts deforming. Figure 6.1b is a graph of the dissipation rate [m^2s^{-3}] of the droplet at the initial breakage plotted versus the mother droplet diameter [mm]. The dissipation rate at breakage using the initial breakage definition is determined at the point of the breakup of the mother droplet.

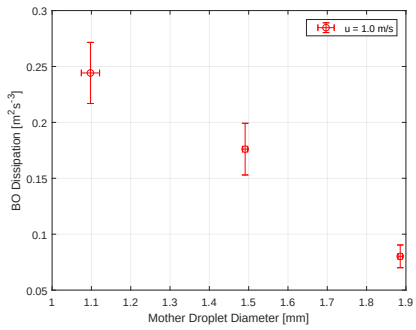

(a) Breakage oscillation (BO) dissipation rate [m^2s^{-3}] versus the mother droplet diameter [mm] with the 95 % confidence interval.

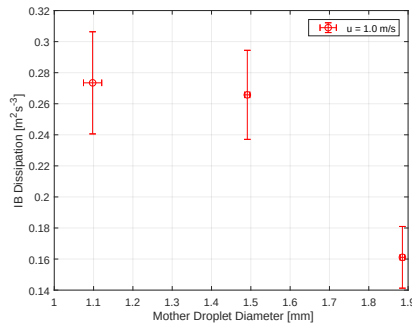

(b) Dissipation rate [m^2s^{-3}] at breakage (IB definition) versus the mother droplet diameter [mm] with the 95 % confidence interval.

Figure 6.1

Both figures imply that the larger mother droplets break at a lower dissipation rate than the mother drops with a smaller diameter. The values of the dissipation rate at the start of the breakage oscillation and at the point of breakage are similar. Additionally, the error in the dissipation rate is quite large. Due to the larger error, it is difficult to conclude that the rate error is any different for the mother droplets at the start of the BO and at the point of breakage.

6.2 Breakage Time

Andersson and Andersson [21] reported a breakage time of 10.9 ms for Octanol oil droplets with a diameter of 1 mm. Their definition of the breakup time is not presented, and the results are thus, difficult to compare with. Solsvik and Jakobsen [29] found the drop breakup time to be increasing with the mother droplet size. The breakage times were found for petroleum oil drops to be 15 ms, 20 ms, and 35 ms for drops of 1 mm, 1.5 mm, and 2 mm respectively. For octanol drops of the same size, the breakage times were 20 ms, 40 ms and 60 ms. Nacthigall [28] found the breakup time using two definitions for petroleum oil droplets. The breakage time was found to be 34.7ms with the original definition and 14.7ms using the new definition.

There is a large variation in the reported breakage times from previous experiments. In addition, the reported breakage times from other literature can be difficult to compare to the breakage times obtained from the experiments performed in this thesis, due to the differences in the experimental setup and definitions of the breakage.

Table 6.1 presents the droplet breakage times with the standard deviation for mother drops with a diameter of 1.10 mm, 1.49 mm, and 1.88 mm. The breakage times are presented using both definitions of breakage, the initial breakup time and the cascade breakup time.

D [mm]	IB time [s]	CB time [s]
1.10 ± 0.133	0.0225 ± 0.0100	0.0327 ± 0.0166
1.49 ± 0.0345	0.0286 ± 0.00970	0.0393 ± 0.0178
1.88 ± 0.0365	0.0485 ± 0.0176	0.0836 ± 0.0537

Table 6.1: Breakage time as a function of mother droplet size with a 95% confidence interval.

The overall trend reported in previous work is that there is an increase in the breakage time with an increasing mother droplet size. This trend can also be spotted for the results presented in Table 6.1. The results are also displayed in Figure 6.2 for the initial breakage definition.

By definition, the cascade breakup time is longer than the initial breakup time. The increase from the initial breakage time to the cascade breakage time definitions are 45%, 37% and 72% for the increasing mother drop sizes.

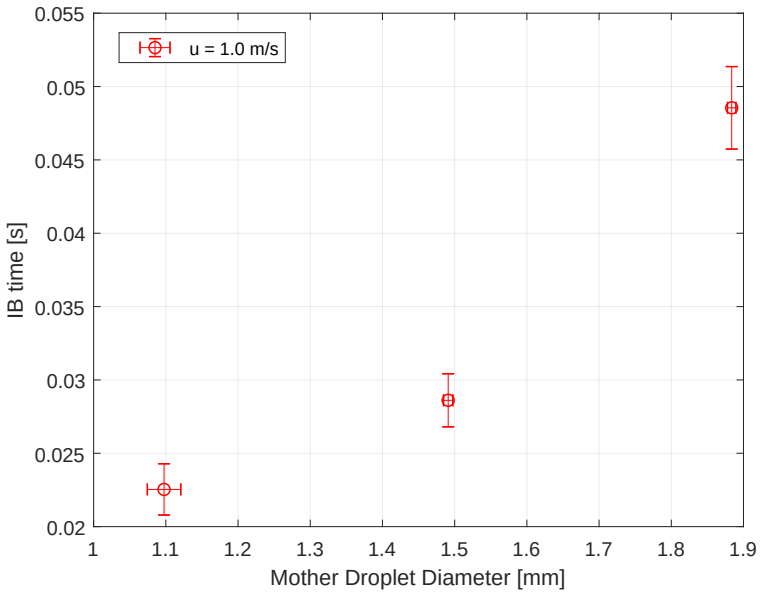

Figure 6.2: Initial breakage time, t_B [s], as a function of mother droplet diameter, D [mm] plotted with a 95 % confidence interval.

The confidence intervals in the results are reasonably small. The largest error in the statistical analysis lies within the performance of the experiments and the image processing. The frame rate of the camera imposes an error for the determination of the breakage time. However, there is a large difficulty in determining when a droplet actually breaks, in terms of the image quality, the lighting and the contrast between the drops and the background, and that the frame rate is not the erroneous factor. Even more so, is the determination of the start of the breakage under a question of doubt. The problem with the start of the breakage is the difficulty to be consistent in every single breakage. The criteria for when to determine when a droplet starts being unstable is discussed in Appendix Appendix C, but even when using these criteria, the start of the breakage can be interpreted in many different ways.

Figure 6.3 shows how the breakage time, using the initial breakage definition, varies with the horizontal position in the channel where the droplet breaks. The figure shows that the breakage time decreases with the distance from the center. The breakage channel, as described in section 4.1, is 30 mm wide. Thus, by defining the center of the channel to be at 0, the channel wall will be at 15 mm. The horizontal position is the droplet height in the channel when the droplet breakage is initialized, i.e. where the droplet starts oscillating.

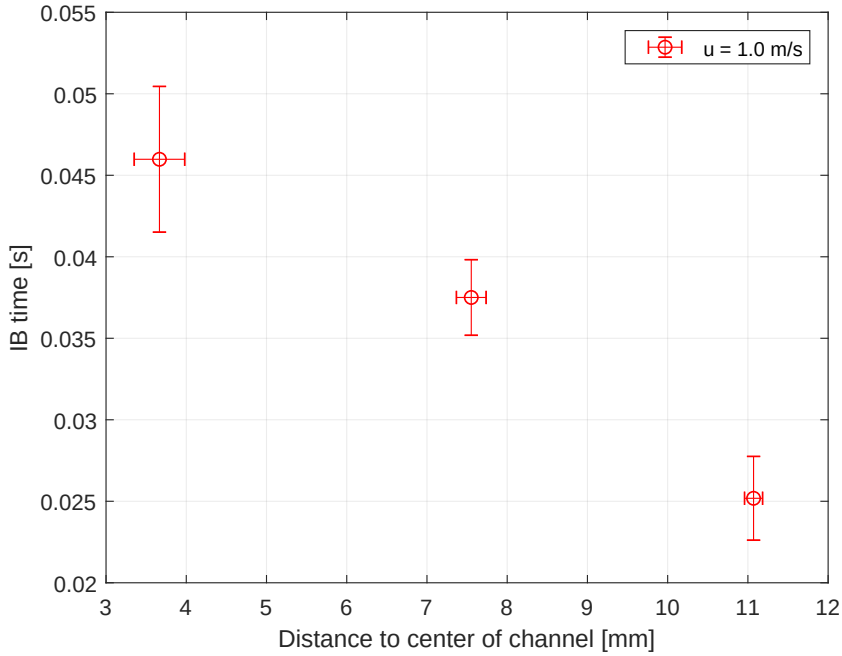

Figure 6.3: IB time [s] plotted as a function of the mother droplet's distance from the centre of channel at the point of breakage. The center of the channel is at 0 mm and the channel walls at either side of the center is at 15 mm.

Figure 6.3 implies that there is a decrease in the breakage time for droplet breaking closer to the wall relative to the droplets breaking in the center. The dissipation rate is higher closer to the wall than in the center. However, this graph illustrated the position of the droplet at the point of breakage. The droplet might have been at a different position when the droplet breakage was initiated.

6.3 Breakage Probability

The breakage probability was estimated as the fraction of observed droplets that broke relative to all the observed droplets. The breakage probability is not influenced by the definition of the breakage. The breakage probability was found to be somewhat increasing with increasing mother droplet area. The breakage probabilities, p_B, for droplets with a diameter, D, is presented in Table 6.2. A standard deviation is not included, because there is no spread in the data. Furthermore, since the breakage probability is estimated by all the data, and thus is calculated from a larger data set than the other variables.

D [mm]	p_b [-]
1.10	0.236
1.49	0.341
1.88	0.345

Table 6.2: Breakage probability, p_B, for droplets of varying droplet diameter, D, in a continuous water flow at 1.0 m/s.

The trend of a monotonous increase breakage probability with an increasing mother droplet size is consistent with what is the expected behavior of the droplets.

Furthermore, there is an increase in the breakage probability for a higher velocity of the water. At a velocity of the continuous phase of 1.5 m/s, all the analyzed droplets were observed to break. This may be explained by the greater turbulent energy dissipation at higher velocities, which will increase the degree of deformation experienced by the drops. This will lead to an increased probability for breakage.

6.4 Breakage Frequency

The breakage frequency, b, is included in the population balance equation and models for the breakage frequency presented by Coulaloglou and Tavlarides [3] and Martínez-Bazán [15]. Maaß and Kraume [27] presented the breakage frequency for their experimental setup using toluene and petroleum oil. Toluene was found to have a breakup frequency of 175 s^{-1} and 75 s^{-1} for mother droplets with a diameter of 1 mm and 2 mm. The breakage frequency for petroleum oil drops of similar size was reported to be 120 s^{-1} and 80 s^{-1}.

The breakage frequencies found in these experiments are presented in Table 6.3. The breakage frequency is calculated using both the breakage time with the initial breakage definition and cascade breakage definition.

D [mm]	b with IB-time [s^{-1}]	b with CB-time [s^{-1}]
1.10	10.5	7.22
1.49	11.9	8.68
1.88	7.11	4.13

Table 6.3: Breakage frequency, b, for droplets of varying droplet diameter, D, in continuous water flow at 1.0 m/s. The breakage frequency is calculated using the breakage time based on the initial breakage and cascade breakage definition.

The breakage frequency reported by Maaß and Kraume are significantly higher than those reported in these experiments. This might be due to the differences in the experimental setup, resulting in a significantly lower the breakage time and a higher probability of breakage.

6.5 Daughter Numbers and Sizes

Andersson and Andersson [21] reported that a binary breakage for the initial breakage was not probable for droplets. Solsvik et al. [11] proposed that an increased frame rate would give a higher probability of a binary breakage. This is in agreement with results presented in this thesis.

The results of the statistical analysis show that the initial breakage always is binary. Typically, breakage commences with a round and stable droplet. Then, due to interactions with a turbulent vortex, the droplet starts deforming. The deformation results in an elongated droplet, thin and threadlike in the center, with a round shape towards the ends. A common case is that this deformed droplet breaks into a smaller rounder droplet and a larger, more deformed droplet. The larger droplet is probable to break into multiple daughters shortly after the initial breakage.

Figure 6.4 shows a typical breakage sequence for a breakage. After deformation, the initial breakage is binary breakage, resulting in two daughter droplets. One of the droplets is strongly deformed and breaks into two new daughters. The time difference between the two daughter droplets in Figure 6.4b and Figure 6.4c is 0.75 ms. A camera with a lower frame rate than 4000 fps could result in breakages of this sort to be interpreted as ternary breakage, rather than a binary breakage.

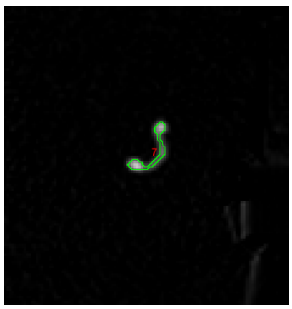

(a) A heavily deformed mother droplet just before breakage.

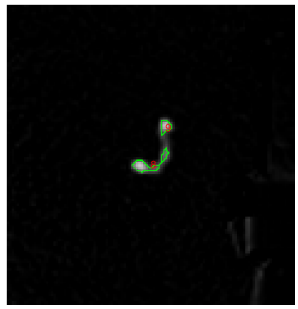

(b) Two daughter droplets after the initial breakage. One daughter is smaller and stable. The other daughter is larger and deformed.

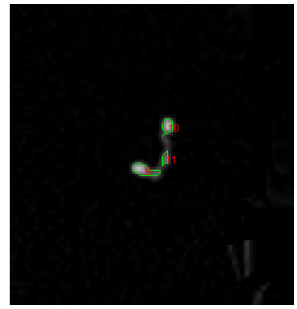

(c) The larger, deformed daughter droplet has broken into two new daughter droplets.

Figure 6.4: Typical breakage sequence for a cascade breakage.

As previously discussed, the initial breakage always resulted in two daughters. Using the cascade breakage definition, the average number of daughters is used as an estimation of the daughter number. The experimental results suggest that there is a small increase in the number of daughters with increasing mother droplet size, as presented in Figure 6.5.

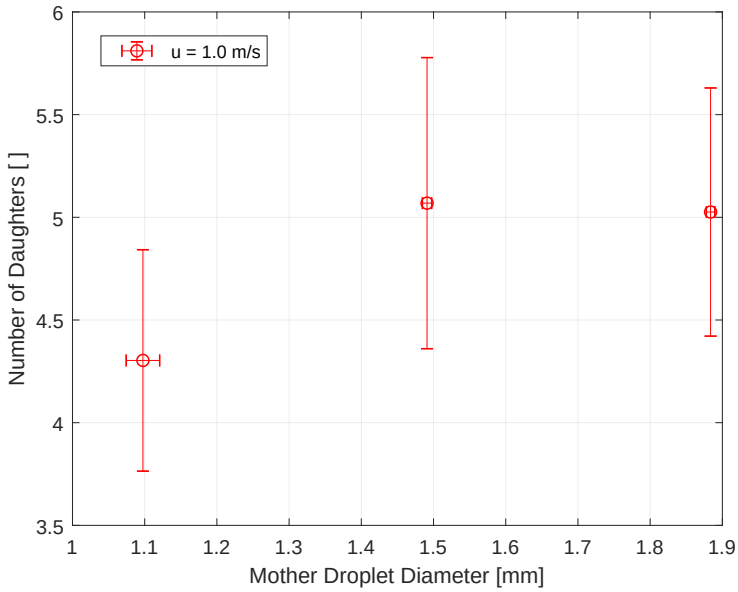

Figure 6.5: Number of daughters in the final distribution [-] as a function of mother droplet diameter [mm]. The velocity of the continuous phase was 1.0 m/s.

The error in the number of daughters is large. The final distribution has been observed to include between 2 and 10+ daughter droplets. Breakages of droplets hitting the channel walls are observed to produce a larger number of daughter droplets than droplet breakages occurring in the center of the channel. To minimize the error, the number of breakages in the data set used in the statistical analysis should be larger.

There is also a possibility that the image analysis provides an error to the obtained results. In order to execute the tracking of the droplets throughout the channel, a background image is subtracted from the frames, resulting in, a black background and with the detected droplets as lighter dots on the image. This process is sensitive to the lighting in the channel and the contrast between

the droplets and the background. When the contrast between the droplets and background is larger, it is easier to deduce a correct representation the droplets on the image. This is relatively straight-forward for larger droplets - they appear darker than the smaller droplets. The smaller droplets, however, and droplets during and after a breakage, appear lighter on the images and might disappear on the resulting binary image. For breakages with a large number of small daughter drops in the final distribution, the reported number of daughters might be incorrect because the drops disappear on the tracking.

Maaß et al. [9] concluded that the common assumption of a Gaussian daughter droplet size distribution could not be supported. They suggested that a bimodal or a bell-shaped distribution would be a suitable model for the daughter droplet distribution. A $\cup$-shaped daughter distribution can be justified by the fact that symmetric binary breakage requires more energy surface energy [35]. $\cap$-shaped daughter distributions imply that the surface energy is a negligible effect on the droplet breakage compared to other types of energies. This is comparable to the results reported by Zaccone et al. [24].

Figure 6.6 displays the final daughter drop size distribution obtained in these experiments, illustrated as a histogram with volume fraction of the mother droplet on the x-asis. The final daughter distribution includes all the daughter drops when the cascade event is concluded. The daughter drop size distribution is plotted for different mother droplet sizes, D = 1.10 mm, 1.49 mm and 1.88 mm.

The daughter drop size distribution is presented as a volume fraction of the mother droplet to account for the differences in mother drop sizes. Looking at the x-axis in the graphs in Figure 6.6, it may be observed that some daughter droplets had a volume fraction above 1. This would imply that some of the daughter droplets are larger than the mother droplet, which, in reality, is not possible.

A volume fraction larger than 1 can be explained by the fact that when the breakage occurs and the daughter drops are created, they are heavily deformed. A strong deformation will result in a higher estimated area of the drops. Since the volume of the droplets is based on the detected droplet area from the image analysis, the estimated volume for the deformed droplets will be too high. This may cause an increased volume fraction and would mean that the some of the largest droplets in the daughter size distribution are, in fact, smaller than they appear in the distribution shown in Figure 6.6. The smaller droplets, however, are usually not deformed, and the estimated volume fraction can be assumed to be more precise.

Due to the issues with the estimation of the droplet size distribution related to the image processing, the distribution can be assumed to need some improvements. The improvements should be directly related to the image processing, to find better methods to estimate the droplet sizes.

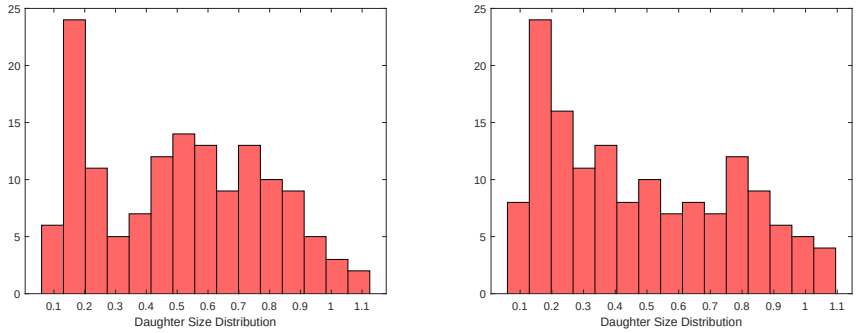

(a)

(b)

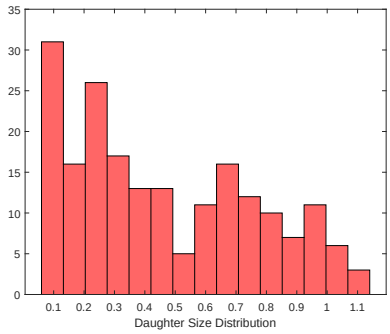

(c)

Figure 6.6: Daughter drop size distribution illustrated as a histogram with the volume fraction for mother droplets of varying size.
(a) D = 1.10 mm, (b) D = 1.49 mm and (c) D = 1.88 mm

The distribution presented here shows a trend of having a higher probability for a volume fraction between 0.1 an 0.3 than a volume fraction between 0.4 and 0.7. This is consistent with the conclusion of Maaß et. al that a Gaussian assumption cannot be supported. However, the distribution is not similar to a bimodal distribution, due to the low number of larger drops. This might be due to a large number of wall breakups, resulting in many small drops.

7 Conclusions

In this work, single droplet breakage has been studied in a two-phase turbulent flow. The study has included multiple steps, including carrying out experiments in the laboratory, performing image analysis to videos of droplets and statistical analysis of the obtained data set. The breakage time, breakage probability, breakage frequency, number of daughters and the daughter size distribution of a single droplet breakage were estimated and compared to existing models of droplet breakup.

Two definitions of droplet breakage are considered. The initial breakage definition defines each individual breakage as an independent event and the cascade breakage definition includes all the breakages until all the daughter droplets stabilize. The results are summarized below:

- The breakage times, t_B for mother droplets of a diameter of 1.098mm, 1.491mm and 1.884mm were found to be 0.0225ms, 0.0286ms, and 0.0485ms, respectively, using the initial breakage definition. The breakage times found with the cascade breakage definition were 45 %, 37 % and 72 % larger than the initial breakage time definition. The breakage times were longer than those reported in literature for similar experiments, but are different to compare due to the differences in the experimental setup and definition of breakage.

- Breakages occurring closer to the channel wall were found to have a shorter breakage time, than in the center of the channel.

- The breakage probabilities, p_B were calculated to be 0.236, 0.341 and 0.345 for droplets with a diameter of 1.098mm, 1.491mm and 1.884mm. Existing literature has reported a higher breakage probability than the probabilities reported in this thesis.

- The breakage frequencies, b, was estimated using existing models to be $10.48s^{-1}$, $11.92s^{-1}$ and $7.113s^{-1}$. Due to the long breakage time and the low breakage probability, the breakage frequency is significantly lower than reported in similar experiments.

- Using the initial breakage definition, all the observed breakages were found to be binary. Using the cascade breakage definition, the number of daughters had a large error due to the small size of the data set and the daughter size distribution had a larger error due to the image analysis.

- The experimental setup in the lab made it possible to produce a large number of observed droplet breakages. The image analysis, however, is time consuming and should be made more efficient. This way, it would be

possible to obtain a larger data set to reduce the error in the measurements of number of daughters and daughter distribution.

8 Future work

The process of analyzing droplet breakage videos is a time-consuming task. It can take up to two hours to complete a full image analysis of a single breakage video. Future work on this study will include more analysis of droplet breakage videos. A larger database of processes droplet breakage videos will mean that it will be easier to compare the results with existing literature and see trends, in particular for the number of daughter droplets and the daughter drop size distribution.

Further experimental investigations may involve running and recording droplet breakage experiments with syringes of varying diameters to achieve a broader mother droplet size distribution. Also, different types of oils may be used to look at the effects of the viscosity of the disperse phase on the droplet breakage.

By using syringes that differ in the inner diameter of the needle, it will be possible to create mother droplets with a range of diameters. By having a larger range of diameters of the mother droplets, any trends will be easier to spot and the results will be more comparable with existing literature.

In order to minimize the workload, but still not compromise on the result and the confidence intervals in the mean value of the measured results, an analysis of the required amount of measurements is necessary. For an increasing amount of measurements, the confidence interval will decrease as a function of the inverse of the square root of the number of measurements. By knowing the number of droplet breakages that are necessary to achieve the desired confidence interval, it is possible to reduce the number of experiments and the workload of analyzing the droplet breakage videos.

References

1. Andersson, B., Andersson, R., Håkansson, L., Mortensen, M., Sudiyo, R. & van Wachem, B. *Computational Fluid Dynamics for Engineers* (Cambridge University Press, 2011).
2. Solsvik, J., Tangen, S. & Jakobsen, H. A. On the constitutive equations for fluid particle breakage. *Reviews in Chemical Engineering* **29,** 241–356 (2013).
3. Coulaloglou, C. A. & Tavlarides, L. L. Description of interaction processes in agitated liquid-liquid dispersions. *Chemical Engineering Science* **32,** 1289–1297 (1977).
4. Solsvik, J., Skjervold, V. T., Han, L., Luo, H. & Jakobsen, H. A. A theoretical study on drop breakup modeling in turbulent flows: The inertial subrange versus the entire spectrum of isotropic turbulence. *Chemical Engineering Science* **149,** 249–265 (2016).
5. Hulburt, H. M. & Katz, S. Some problems in particle technology: A statistical mechanical formulation. *Chemical Engineering Science* **19,** 555–574 (1964).
6. Ramkrishna, D. *Population balances : theory and applications to particulate systems in engineering* (Academic Press, San Diego, Calif, 2000).
7. Luo, H. *Coalescence, breakup and liquid circulation in bubble column reactors* Trondheim, 1993.
8. Luo, H. & Svendsen, H. F. *Theoretical model for drop and bubble breakup in turbulent dispersions* **5,** 1225–1233. doi:10.1002/aic.690420505 (American Institute of Chemical Engineers, New York, 1996).
9. Maaß, S., Buscher, S., Hermann, S. & Kraume, M. Analysis of particle strain in stirred bioreactors by drop breakage investigations. *Biotechnology Journal* **6,** 979–992 (2011).
10. Jakobsen, H. A. *Chemical Reactor Modelling - Multiphase Reactive Flows* 807–858 (Springer, 2014).
11. Solsvik, J., Maaß, S. & Jakobsen, H. A. Definition of the Single Drop Breakup Event. *Industrial and Engineering Chemistry Research* **55,** 2872–2882 (2016).
12. Han, L., Luo, H. & Liu, Y. A theoretical model for droplet breakup in turbulent dispersions. *Chemical Engineering Science* **66,** 766–776 (2011).
13. Han, L., Gong, S., Li, Y., Ai, Q., Luo, H., Liu, Z. & Liu, Y. A novel theoretical model of breakage rate and daughter size distribution for droplet in turbulent flows. *Chemical Engineering Science* **102,** 186–199 (2013).

14. Han, L., Gong, S., Ding, Y., Fu, J., Gao, N. & Luo, H. A. Consideration of low viscous droplet breakage in the framework of the wide energy spectrum and the multiple fragments. *AIChE Journal* **61,** 2147–2168 (2015).

15. Martínez-Bazán, C., Montañés, J. L. & Lasheras, J. C. On the breakup of an air bubble injected into a fully developed turbulent flow. Part 1. Breakup frequency. *Journal of Fluid Mechanics* **401,** 157–182 (1999).

16. Martinez-Bazan, C., Montanes, J. & Lasheras, J. On the breakup of an air bubble injected into a fully developed turbulent flow. Part 2. Size PDF of the resulting daughter bubbles. *Journal Of Fluid Mechanics* **401,** 183–207 (1999).

17. Solsvik, J., Skjervold, V. T. & Jakobsen, H. A. A bubble breakage model for finite Reynolds number flows. *Journal of Dispersion Science and Technology* **38,** 973–978 (2017).

18. Pilch, M. & Erdman, C. A. *Use of breakup time data and velocity history data to predict the maximum size of stable fragments for acceleration-induced breakup of a liquid drop* 1987. doi:10.1016/0301-9322(87)90063-2.

19. Galinat, S., Masbernat, O., Guiraud, P., Dalmazzone, C. & Noik, C. Drop break-up in turbulent pipe flow downstream of a restriction. *Chemical Engineering Science* **60,** 6511–6528 (2005).

20. Galinat, S., Garrido Torres, L., Masbernat, O., Guiraud, P., Risso, F., Dalmazzone, C. & Noik, C. Breakup of a drop in a liquid–liquid pipe flow through an orifice. *AIChE Journal* **53,** 56–68 (2007).

21. Andersson, R. & Andersson, B. On the breakup of fluid particles in turbulent flows. *Aiche Journal* **52,** 2020–2030 (2006).

22. Andersson, R. & Andersson, B. Modeling the breakup of fluid particles in turbulent flows. *Aiche Journal* **52,** 2031–2038 (2006).

23. Maaß, S., Gäbler, A., Zaccone, A., Paschedag, A. R. & Kraume, M. Experimental investigations and modelling of breakage phenomena in stirred liquid/liquid systems. *Chemical Engineering Research and Design* **85,** 703–709 (2007).

24. Zaccone, A., Gäbler, A., Maaß, S., Marchisio, D. & Kraume, M. Drop breakage in liquid–liquid stirred dispersions: Modelling of single drop breakage. *Chemical Engineering Science* **62,** 6297–6307 (2007).

25. Diemer, R. B. & Olson, J. H. A moment methodology for coagulation and breakage problems: Part 3—generalized daughter distribution functions. *Chemical Engineering Science* **57,** 4187–4198 (2002).

26. Maaß, S., Wollny, S., Sperling, R. & Kraume, M. Numerical and experimental analysis of particle strain and breakage in turbulent dispersions. *Chemical Engineering Research and Design* **87,** 565–572 (2009).

27. Maaß, S. & Kraume, M. Determination of breakage rates using single drop experiments. *Chemical Engineering Science* **70,** 146–164 (2012).

28. Nachtigall, S., Zedel, D. & Kraume, M. Analysis of drop deformation dynamics in turbulent flow. *Chinese Journal of Chemical Engineering* **24,** 264–277 (2016).

29. Solsvik, J. & Jakobsen, H. A. Single drop breakup experiments in stirred liquid-liquid tank. *Chemical Engineering Science* **131,** 219–234 (2015).

30. Wheeler, A. J. & Ahmad, R. G. *Introduction to engineering experimentation* Boston, 2010.

31. Box, G. E. P., Hunter, J. S. & Hunter, W. G. *Statistics for experimenters : design, innovation, and discovery* Hoboken. N.J, 2005.

32. Blischke, W. R. & Murthy, D. N. P. in *Wiley Series in Probability and Statistics* 749–762 (John Wiley & Sons, Inc., Hoboken, NJ, USA, 2011). doi:10.1002/9781118150481.app3.

33. Herø, E. H., Forgia, N. L., Solsvik, J. & Jakobsen, H. A. Determination of Breakage Parameters in Turbulent Fluid-Fluid Breakage. *Chemical Engineering & Technology* **42,** 903–909 (2019).

34. La Forgia, N., Herø, E. H., Solsvik, J. & Jakobsen, H. A. Dissipation rate estimation in a rectangular shaped test section with periodic structure at the walls. *Chemical Engineering Science* **195,** 159–178 (2019).

35. Wang, T., Wang, J. & Jin, Y. A novel theoretical breakup kernel function for bubbles/droplets in a turbulent flow. *Chemical Engineering Science* **58,** 4629–4637 (2003).

Appendices

A Maintenance of Experimental Setup

A.1 Drying

To avoid growth of unwanted microorganisms in the pipes, the pipes are opened once every week to remove water from the pipes when the apparatus is not in use. This process is done after a session of experimental runs are finished, and most of the water is pumped back into the water tank and the valve is shut. A metal cover is removed and the pipe is emptied of excess water using a multi-purpose vacuum cleaner. The pipe is left open until next experimental run to ensure that the inside of the pipes dry.

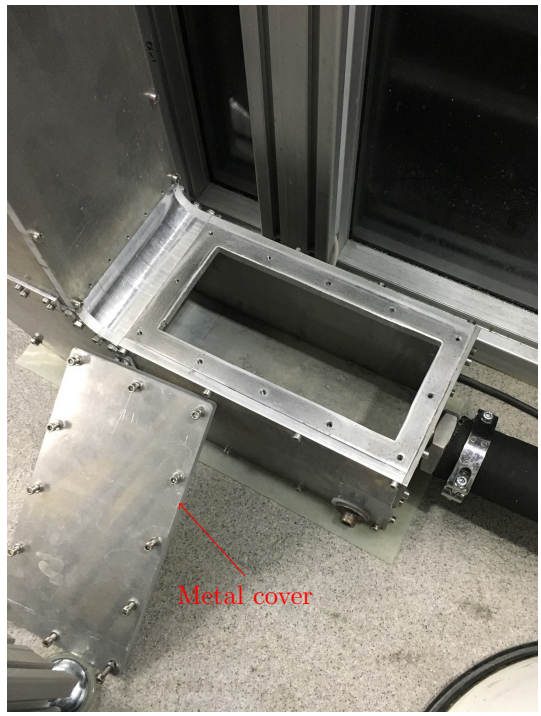

Figure A.1: This metal cover is removed to remove any water left in the tank after shutdown and letting the pipes dry

A.2 Cleaning

Cleaning of the experimental setup is done by emptying the apparatus for water. The water is removed opening a valve in the bottom of the water reservoir tank, releasing the water in the tank into a drain. After the tank is emptied, any excess water in the pipes is removed using a multi-purpose vacuum cleaner. Any pipelines that can be unscrewed from the circuit is removed and cleaned separately using distilled water. The water tank is cleaned with water and a stiff-haired round brush. The breakage channel is the most challenging part to clean, but it can be done by using a slim round brush and water. It is important to make sure that any hairs from the brush used in the cleaning is not stuck anywhere in the breakage channel, as it can be detected on the camera as disturb the image analysis.

A.3 Preparation of Oil and Refilling the Syringe

When the oil level in the syringe is low, new oil for the experiments have to be prepared. The syringe is removed from its stand and the needle connected to the syringe by a pipe is unscrewed from the droplet generation channel. The rest of the process is executed under a fume hood. The syringe, the pipe and the needle are both cleaned used de-ionized water. The oil is prepared by mixing the oil with a coloring agent, Sudan Black B, using a magnetic stirrer. The prepared oil is then injected into the syringe and put back into the apparatus.

A.4 Refilling of Water

Every couple of weeks, the water reservoir tank is emptied of water and refilled with new de-ionized water. The aim of refilling the tank with de-ionized water is to remove any microorganisms, dust or hairs that might have been collected in the circuit throughout the running of the experiments. These particles are unwanted in the system, because they can be detected as droplets of the camera and thus hindering the detecting the actual oil droplets and cause worse quality droplet breakage images. The supply of de-ionized water is short. The de-ionized water is tapped from a central storage into large plastic containers to be stored until refilling, to ensure a quicker refilling of the tank, see Figure A.2.

Figure A.2: Plastic containers used for storage of de-ionized water before emptying and refilling the water reservoir tank in the experimental apparatus.

B Considerations related to the Experiments: 'data.txt'

Below, an example data-text file is presented. The data files include information considering the camera settings, syringe pump settings and temperature in the continuous phase.

FrameRate	4000
InfusingRate	18
Width1	1024
Height1	1024
Width2	1024
Height2	1024
Q[m3/s]	1.067806E−3
Q[**std**]	9.811631E−6
u	1.483064E+0
RoiWidth1	635
RoiHeight1	1024
Roi_xpos1	422
Roi_ypos1	0
RoiWidth2	623
RoiHeight2	1024
Roi_xpos2	409
Roi_ypos2	0
Cam1_pos	67
Cam2_pos	238
Temp	24

C Considerations related to the Image Analysis: Stability of a Droplet

The stability of a drop is of crucial importance in the image analysis, particularly for the determination of the start of the breakage oscillation, BO, and for the determination of the end of a breakage event.

In order to be consistent in the determination of the stability of the drop, a criterion for droplet stability was defined. A perfectly spherical droplet is interpreted to be in its most stable form, due to a minimization of the surface energy of the drop. Thus, when the drop starts deforming, the droplet becomes less stable.

There are several methods to investigate the roundness of a droplet. All methods are based on the frames from the droplet videos. Since the images of the droplets in the breakage channel are projections of a three dimensional system onto a two dimensional plane, it is not possible to confirm the droplets' three dimensional shape.

It is assumed that the if the droplet is circular in a two dimensional plane, it is spherical in three dimensions. This might not always be a good assumption, as the droplet can deform in any direction and the cameras can only detect deformation in the plane captured on camera.

- Large variations in the droplet area can be interpreted as a deformation of a droplet and thus, a destabilization of the droplet. This can be observed as oscillations in a plot of the droplet area as function of the frame number, as shown in Figure C.1.

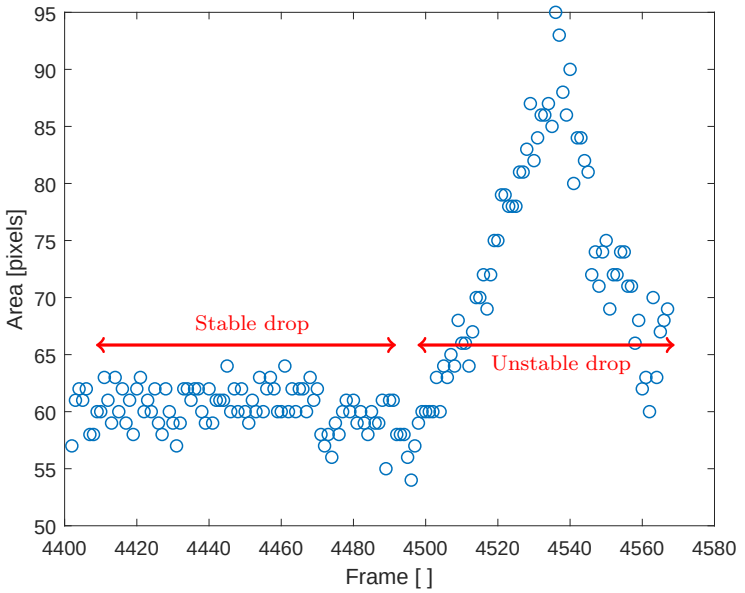

Figure C.1: Droplet area plotted chronologically by the frame number. This graph can be used to find droplet deformation. An increase in the droplet area can imply the droplet is under deformation.

The figure illustrates that the droplet area is constant between frame 4400 and 4500, prior to a rapid increase in the droplet area from frame 4500. The deviation from the constant droplet area is an indication of droplet deformation, and thus, destabilization.

This technique is a good method to see identify droplet deformation, but is not the most precise when it comes to determining the point where the destabilization starts.

- A deformation plot is a very useful tool to find the point where the droplet starts deforming and destabilizing. If the deformation is larger than 0.1, the droplet is defined to be under deformation. Figure C.2 illustrates an example plot of the deformation for a droplet that initially is stable and starts deforming around 4480.

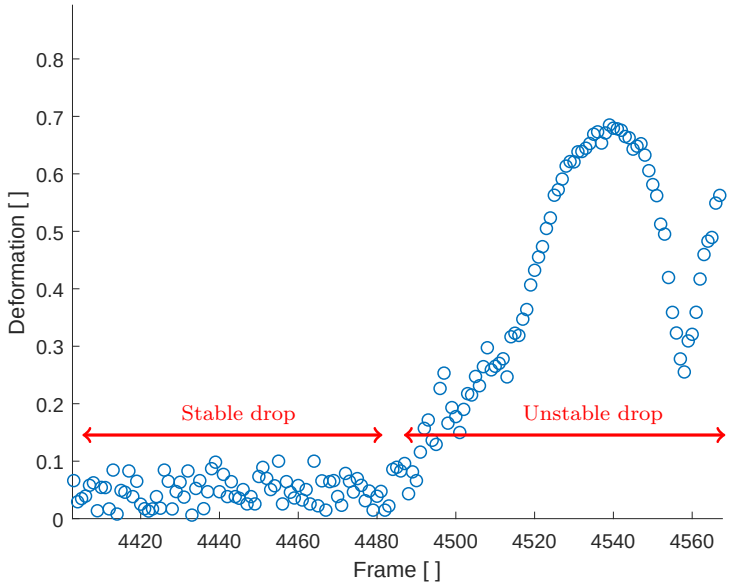

Figure C.2: Droplet deformation plotted chronologically with the frame number. This plot is often used to find the point where the droplet starts deforming.

- Finally, the stability of a droplet can be confirmed by looking the droplet on the images to see if a droplet appear circular. Figure C.3 illustrates the different between a circular, stable droplet and a droplet that is unstable and under deformation.

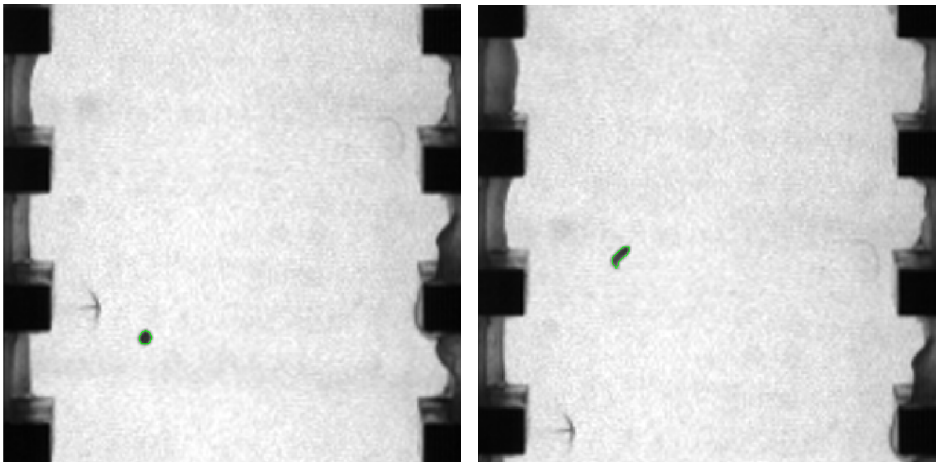

(a) Droplet appears very circular and can be defined as stable.

(b) Droplet is deformed and therefore not stable.

Figure C.3

Studying the droplets on the images is frequently combined with the two previously mentioned methods for determining the stability of a droplet. By first using an area plot or a deformation plot to find where the droplets are deformed and then looking at relevant frames to confirm the hypothesis.

SECTION 1. Identification of the substance/mixture and of the company/undertaking

1.1. Product identifier

Trade name : Sudan black B

1.2. Relevant identified uses of the substance or mixture and uses advised against

Use : For professional use only.

1.3. Details of the supplier of the safety data sheet

Company identification : RAL DIAGNOSTICS S.A.S.
Site Montesquieu
33651 MARTILLAC CEDEX France
Tel : +33 (0) 5 57 96 04 04 Fax : +33 (0) 5 57 96 04 05
www.ral-diagnostics.com
Email: fds@ral-diagnostics.fr

1.4. Emergency telephone number

Emergency phone nr : ORFILA : +33 (0) 1 45 42 59 59

SECTION 2 Hazards identification

2.1. Classification of the substance or mixture

Classification EC 67/548 or EC 1999/45

Classification : Not classified.

Hazard Class and Category Code(s), Regulation (EC) No 1272/2008 (CLP)

Not regulated.

2.2. Label elements

Labelling Regulation EC 1272/2008 (CLP)

- **Hazard pictograms** : None.
- **Signal words** : None.
- **Hazard statements** : None.
- **Precautionary statements**

None.

2.3. Other hazards

Other hazards : None under normal conditions.

SECTION 3 Composition/information on ingredients

Substance / Preparation : Substance.

This product is not considered to be hazardous and does not contain hazardous components.

Substance name		Value(s)	CAS nr	EINECS nr	EC index	REACH	Classification
Sudan black B	:	100 %	4197-25-5	224-087-1	-----	----	Not classified. (DSD/DPD) --- Not classified. (GHS)

C.I. (colour index) : 26150
RETECS# : SD4431500

SECTION 4. First aid measures

4.1. Description of first aid measures

First aid

- **Inhalation** : Take victim to fresh air. Obtain medical attention if breathing difficulty persists.
- **Skin contact** : Seek medical attention if ill effect or irritation develops.
- **Eye contact** : Rinse with water. Seek medical attention if irritation develops.
- **Ingestion** : Rinse mouth. Seek medical attention if ill effect develops.

4.2. Most important symptoms and effects, both acute and delayed

- **Inhalation** : Dust of the product, if present, may cause respiratory irritation after an excessive inhalation exposure. Dry throat. Headache.
- **Skin contact** : Not expected to present a significant skin hazard under anticipated conditions of normal use.
- **Eye contact** : Not expected to present a significant eye contact hazard under anticipated conditions of normal use.
- **Ingestion** : Must not come into contact with food or be consumed. No significant signs or symptoms indicative of any adverse health hazard are expected to occur as a result of ingestion.

4.3. Indication of any immediate medical attention and special treatment needed

No data available.

SECTION 5. Fire-fighting measures

5.1. Extinguishing media

Extinguishing media : All extinguishing media can be used.

5.2. Special hazards arising from the substance or mixture

Special exposure hazards : Carbon oxides Nitrogen oxides.

5.3. Advice for fire-fighters

Flammable class : Not combustible.

Protection against fire : Do not enter fire area without proper protective equipment, including respiratory protection.

SECTION 6. Accidental release measures

6.1. Personal precautions, protective equipment and emergency procedures

Personal precautions : Equip cleanup crew with proper protection. Avoid dust production. Respiratory protection equipment may be necessary. Ensure adequate ventilation.

6.2. Environmental precautions

Environmental precautions : Prevent entry to sewers and public waters.

6.3. Methods and material for containment and cleaning up

After spillage and/or leakage : Sweep or shovel spills into appropriate container for disposal. Dispose in a safe manner in accordance with local/national regulations.

6.4. Reference to other sections

See Heading 8.

SECTION 7. Handling and storage

7.1. Precautions for safe handling

General : Use good housekeeping practices to avoid rendering dust airborne.

Handling : Handle in accordance with appropriate industrial hygiene and safety procedures. Keep away from food, drink and animal feeding stuffs. Wash hands and other exposed areas with mild soap and water before eat, drink or smoke and when leaving work.

Technical protective measures : Dust extraction (suction)

7.2. Conditions for safe storage, including any incompatibilities

Storage : Keep cool. Store in dry, well-ventilated area. Store in tightly closed containers.

7.3. Specific end use(s)

Not applicable.

SECTION 8. Exposure controls/personal protection

8.1. Control parameters

No data available.

8.2. Exposure controls

Personal protection

• Respiratory protection : When risk assessment shows air-purifying respirators are appropriate, Wear a mask with particle filter type P95 (U.S.) or type P1 (EN143). Use respirators and components tested and approved under appropriate government standards such as NIOSH (US) or CEN (EU).

• Hand protection : Gloves. The selected protective gloves have to satisfy the specifications of EU Directive 89/686/EEC and the standard EN 374 derived from it.

• Skin protection : Wear proper protective equipment. Choose body protection in relation to the dangerousness of the product, its concentration and the amounts used depending on the workstation.

• Eye protection : Goggles. Use equipment for eye protection tested and approved under appropriate government standards such as NIOSH (US) or EN 166(EU).

• Ingestion : When using, do not eat, drink or smoke.

Industrial hygiene : Provide local exhaust or general room ventilation to minimize exposure to dust. Emergency eye wash fountains should be available in the immediate vicinity of any potential exposure.

SECTION 9. Physical and chemical properties

9.1. Information on basic physical and chemical properties

9.1.a. Appearance

Physical state : Cristallin powder.

Colour : Black.

9.1.b. Odour

Odour : Odourless.

9.1.c. Odour threshold

No data available.

9.1.d. pH

No data available.

SECTION 9. Physical and chemical properties (continued)

9.1.e. Melting point / Freezing point

Melting point [°C] : 120 - 124

9.1.f. Initial boiling point - boiling range

No data available.

9.1.g. Flash point

No data available.

9.1.h. Evaporation rate

No data available.

9.1.i. Flammability

No data available.

9.1.j. Explosion limits (lower - upper)

No data available.

9.1.k. Vapour pressure

No data available.

9.1.l. Vapour density

No data available.

9.1.m. Relative density

No data available.

9.1.n. Solubility

Solubility in : Ethyl alcohol. : 30 g/L.

Solubility in water : 0.1 g/L

9.1.o. Partition coefficient : n-octanol / water

No data available.

9.1.p. Auto-ignition temperature

No data available.

9.1.q. Thermal decomposition

No data available.

9.1.r. Viscosity

No data available.

9.1.s. Explosive Properties

No data available.

9.1.t. Oxidising properties

No data available.

9.2. Other information

No data available.

SECTION 10. Stability and reactivity

10.1. Reactivity

No data available.

10.2. Chemical stability

Physico-chemical stability : Stable in normal temperature and pressure conditions.

10.3. Possibility of hazardous reactions

No data available.

10.4. Conditions to avoid

Conditions to avoid : Water. Moisture. Sources of ignition. High temperature.

10.5. Incompatible materials

Materials to avoid : Strong oxidisers. Strong bases.

10.6. Hazardous decomposition products

Hazardous decomposition products : Carbon monoxide. Carbon dioxide. Nitrogen oxides.

SECTION 11. Toxicological information

11.1. Information on toxicological effects

• Acute toxicity

On ingredients

Sudan black B : Rat oral LD50 [mg/kg] : > 2000

• Skin corrosion/irritation : Rabbit. No skin irritation.

• Serious eye damage/irritation : Rabbit. May cause minor eye irritation.

• Respiratory or skin sensitisation : No sensitizing effects known.

• Germ cell mutagenicity : Genotoxicity in vitro - Histidine reversion (Ames) - S. Typhimurium.

• Carcinogenicity : No data available.

• Reproductive toxicity : No data available.

• STOT-single exposure : No data available.

• STOT-repeated exposure : No data available.

• Aspiration hazard : No data available.

• Potential effects on health : No data available.

• Signs and symptoms of exposure : No data available.

SECTION 12. Ecological information

12.1. Toxicity

No data available.

12.2. Persistence - degradability

No data available.

12.3. Bioaccumulative potential

No data available.

12.4. Mobility in soil

No data available.

12.5. Results of PBT and vPvB assessment

SECTION 12. Ecological information (continued)

No data available.

12.6. Other adverse effects

Not release to the environment.

SECTION 13. Disposal considerations

13.1. Waste treatment methods

Disposal : Dispose in a safe manner in accordance with local/national regulations.
Dispose of this material and its container at hazardous or special waste collection point.

SECTION 14. Transport information

14.1. UN number

- **UN No.** : Unregulated.

14.2. UN proper shipping name

- **Proper shipping name** : Unregulated.

14.3. Transport hazard class(es)

- **Hazard Label(s)** : Unregulated.
- **Class** : Unregulated.
- **H.I. nr :** : Unregulated.
- **Classification code** : Unregulated.

14.4. Packing group

- **ADR Packing group** : Unregulated.
- **IMO Packing group** : Unregulated.
- **IATA Packing group** : Unregulated.

14.5. Environmental hazards

- **IMDG-Marine pollution** : Unregulated.

14.6. Special precautions for user

Emergency action in case of accident

- **IMO-IMDG code** : FS : Unregulated.

14.7. Transport in bulk according to Annex II of MARPOL73/78 and the IBC Code

Not applicable.

SECTION 15. Regulatory information

15.1. Safety, health and environmental regulations/legislation specific for the substance or mixture

Ensure all national/local regulations are observed.

EC Classification : Sudan black B
CAS nr :4197-25-5
EINECS nr :224-087-1
EC index :---
REACH :---

15.2. Chemical Safety Assessment

SECTION 15. Regulatory information (continued)

A chemical safety assessment has not been performed.

SECTION 16. Other information

Revision	: 5
Print date	: 8 / 4 / 2013
Further information	: Product intented for professional use only.

The contents and format of this SDS are in accordance with REGULATION (EC) No 453/2010 OF THE EUROPEAN PARLIAMENT AND OF THE COUNCIL.

DISCLAIMER OF LIABILITY The information in this SDS was obtained from sources which we believe are reliable. However, the information is provided without any warranty, express or implied, regarding its correctness. The conditions or methods of handling, storage, use or disposal of the product are beyond our control and may be beyond our knowledge. For this and other reasons, we do not assume responsibility and expressly disclaim liability for loss, damage or expense arising out of or in any way connected with the handling, storage, use or disposal of the product. This MSDS was prepared and is to be used only for this product. If the product is used as a component in another product, this MSDS information may not be applicable.

End of document

RAL DIAGNOSTICS S.A.S.
Site Montesquieu 33651 MARTILLAC CEDEX France
Tel : +33 (0) 5 57 96 04 04 Fax : +33 (0) 5 57 96 04 05
www.ral-diagnostics.com
Email: fds@ral-diagnostics.fr